Spring 2020

Zips Electric - Cooling System

Guan-Bok Kwok
gk64@zips.uakron.edu

The University of Akron

College of Engineering

Senior Design Report

Zips Formula Electric Racing

Cooling System

Fall 2019 – Spring 2020

Advisor: Dr. Daniel Deckler

Team Members:

Guan-Bok Kwok

Brendan O'Donnell

Andrew Thouvenin

Executive Summary

In order to achieve optimal performance, the Zips Electric Racing 2020 electric race car must be properly cooled. The main objective for the design of this cooling system was to ensure efficient cooling of the car's EMRAX® 228 electric motor and Cascadia Motion© PM100 DX power inverter. To accomplish this task, a simple and efficient system was designed to utilize a standard Mishimoto™ CRF450R aluminum dirt bike radiator along with a Davies Craig© EBP40 centrifugal water pump. Other objectives focused on during the design process included weight reduction, data collection, and cost reduction.

Design of the system was based on results obtained from theoretical calculations in parallel with wind tunnel testing. A wind tunnel experiment was designed and conducted at the AEROLAB Open Circuit Low-Speed Wind Tunnel located at The University of Akron. The results were extensively analyzed and provided empirical data essential for the design of the cooling system. Testing was ran at various wind speeds and mounting angles to collect as much relevant data as possible. The data was compared to the theoretical calculations and simulations. Parts of the data was also used to complete predictive models and construct adaptive MATLAB codes for future teams.

Theoretical calculations and models were developed as a base model to validate the accuracy of the test data. Predictive thermal characteristic models were created in Simulink, a graphical MATLAB based modeling environment, with identical boundary conditions as the physical wind tunnel test. Theoretical equations were also derived to determine the maximum thermal input the cooling system would be subjected to. These calculations were combined with system data collected from ZER 19's data acquisition system to formulate more realistic estimates of the potential energy to be absorbed by the cooling system.

A sidepod was designed and adjusted to promote optimal airflow into the radiator via forced convection. The geometry of the sidepod was largely influenced by determining the ideal mounting angle of the radiator to maximize the forward-facing surface area, increasing heat dissipation by forced convection. However, due to budget constraints, the sidepod was redesigned and optimized as simple composite radiator cover plates. Extensive CFD simulations were executed to optimize the airflow channeled by these plates.

During manufacturing, silicone tubing was chosen to optimize the routing of the cooling lines due to its low cost, high flexibility, and suitable thermal resistance. Optimization also resulted in shortening the cooling fluid's route, consequently, the volume of coolant (deionized water) within the system was minimized, and, thus, weight was reduced. Weight was also reduced by increasing the utilization of composite materials throughout the system. Overall system costs were reduced by designing the system to efficiently maximize the outputs of the critical components.

Acknowledgement

We would like to thank Dr. Deckler, Dr. Wang, and Dr. Sawyer for their support on this design project. Assistance from the Zips Combustion Team was also critical, with their extensive design experience to draw from. We'd also like to thank Collins Aerospace for donating essential resources and materials necessary to design, test, and fabricate components.

Table of Contents

Chapter 1: Introduction

1.1 Background

The need of a cooling system in the Zips Electric Racecar is to ensure the motor and inverter don't exceed the maximum operating temperatures. The design was optimized around a radiator and pump that were previously selected to be used in the car. Ideally, these two critical components would be selected after reaching an optimized design.

Theoretical calculations and computer simulations were performed parallel to physical testing to determine the characteristics of the pump and radiator. The manufacturer of the radiator, Mishimoto, does not publish any data for their products making the thermal and geometric properties of the radiator unknowns which needed to be solved as part of the design. In order to reverse engineer the radiator took extensive analysis and simulations to be able to establish confidence in the design.

An effective design of the cooling system would be considered any design which could allow the ZER 2020 vehicle to operate continuously for at least the duration of one full charge. The operational temperature of the drivetrain system is 150°F or 65.5°C, and therefore the effective design must be able to maintain a steady state temperature below this temperature regardless of the power output from the drivetrain.

1.2 Literature Search

For the design, the most important documentation is the FSAE Rules 2020 for formula electric. Rules applying specifically to the cooling subsystem are spread throughout the documentation. Figure 1 shows an example of one such rule applying directly to the cooling system.

T.5.3	**Coolant Fluid**
T.5.3.1	Water cooled engines must use only plain water with no additives of any kind.
T.5.3.2	Coolant for electric motors, accumulators or HV electronics must be one of:
	• plain water with no additives
	• oil

Figure 1. Excerpt from FSAE Rules 2020

In addition, the design report from the ZER 2019 cooling subsystem was referenced as the starting point for all models designed. However, the system from ZER 2019 seemed to be under tested and therefore was overdesigned and gave an opportunity to eliminate components such as the fan and the ductwork.

Extensive research was conducted to determine the correct calculations for the theoretical analysis of the cooling system. Theories from multiple heat transfer and fluids textbooks were referenced to ensure the accuracy of the derived equations. The textbooks are found in the References and short excerpts of the theories used can be found in Appendix B.

1.3 Principles of Operation

The cooling subsystem operates in a simple closed loop configuration. The motor, being more sensitive to thermal effects, is directly downstream of the pump. As the coolant enters the radiator, convective heat transfer occurs from the water to the internal surface of the radiator. The aluminum radiator then transfers heat to the impinging air, again through convection. The airflow is optimized by the addition of panel covers which channel the air into the radiator. The choice to use the specific design of the panel covers came from the CFD analysis which showed the impinging air bypassing the radiator without additional channeling.

The rate of heat transfer into the system by the motor and inverter was from a data set acquired from the ZER 2019 vehicle. Knowledge of the radiator was acquired by testing the system in a wind tunnel at various coolant flow rates and impinging wind speeds. Calculations for heat generated to heat dissipated by cooling system can be seen in figure #XX. The achievable flow rates of the centrifugal pump were tested using a flow meter and a mock configuration of the ZER 2020 vehicle. An assumption was made that the silicone tubing was incapable of transferring heat away from the system i.e. the tubing acted as a perfect insulator. From the Simulink model it was proven this is a valid assumption.

1.4 Product Definition

The prototype design uses an aluminum radiator manufactured by Mishimoto under the generic name X-braced dirt bike radiator. As for the thermal characteristics of the radiator, Mishimoto only claims the ability to perform adequately for the vehicle for which it is manufactured but publishes no technical data. For this reason, end-to-end analysis was performed to reverse engineer the radiator to determine adequacy in the specific application.

The pump used is the EBP40 12V centrifugal pump capable of an output of 40 L/min under unrestricted flow conditions. For the specific application, the pump can deliver a maximum of 11 L/min to the system. The motor and the inverter (EMRAX® 228MV and PM100DX respectively), which provide most of the flow restriction, are part of the drivetrain subsystem and are limited to an 80kW output as per the standards of FSAE. The coolant is forced by the centrifugal pump into the motor and then into the inverter before returning to the radiator exposed to the impinging air. From data sheets provided by the manufacturer of the EMRAX® 228 MV state that the motor's maximum operating temperature is 150°F or 65.5°C and the electrical team decided to implement an automatic shutoff of the vehicle if the temperature reached this condition within the system. For this reason, 65.5°C is used as the baseline for the subsequent tests performed.

The entire system is connected using silicone tubing because in a cost to weight comparison, there are no significant advantages to other materials. Carbon fiber tubing was investigated initially due to its lighter weight and ability to allow heat to leave the system through the tubing itself, but due to the significantly higher cost, difficulty in working and designing a mounting system, and minimal benefits in heat dissipation and weight reduction, there was minimal effort devoted to such a concept.

The entire subsystem is mounted to tabs welded to the chassis. FEA simulations were used to prove that the mounting system is adequate to not only withstand the event of a rollover, but also not cause damage to the chassis as per FSAE rules.

Chapter 2: Conceptual Design

2.1 Design Brief

The cooling system is designed to be capable of dissipating enough heat to allow ZER 2020 vehicle to operate at the maximum power condition. For the motor used in the vehicle, the EMRAX® 228 MV, the maximum output seen from the data acquired from ZER 2019 is 60 kW peak. However, the maximum sustained output of the motor is only 30 kW since many racing events do not stress the ability to produce mechanical power. Any power greater than this 30kW is not shown to be sustained for extended periods of time and not likely to be held for long enough to be an issue for the cooling system to handle. The motor is advertised to have an efficiency of 90% and therefore the cooling system must be able to dissipate at least 3 kW consistently. The wind tunnel test system is given by figure 24. The first test plan was to heat five gallons of water to 66°C and pump the water into the radiator and finally to a cold reservoir. For these tests the water was not circulated through the system. A full test plan can be seen in section 3.6 Wind Tunnel Testing.

For all recorded and presented tests, the condition to terminate the test was after a steady state temperature had been achieved at the outlet. The test had thermocouples to monitor the hot reservoir temperature, internal radiator surface, and outlet temperature of the radiator. From figure 2 and figure 3, it can be seen that as the speed of the vehicle increases, so does the ability to dissipate heat until the vehicle speed increases to 43 mph. However, at the highest speed which corelates to the highest power output the system can dissipate approximately 3.7 kW. Although the system can handle going beyond 50 mph, it is unlikely that this operating point will be sustained for any significant time period due to the design of the race events. From this data set, the team had the confidence to proceed with more appropriate, yet time consuming tests without the need for a redesign.

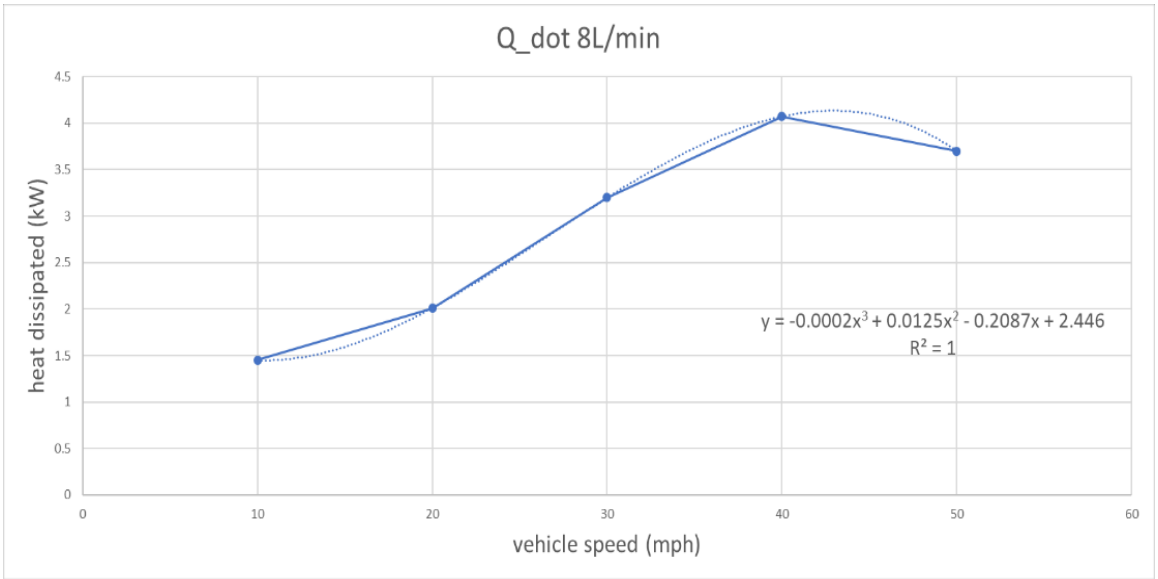

Figure 2 Results of Wind Tunnel Testing at 8 L/min

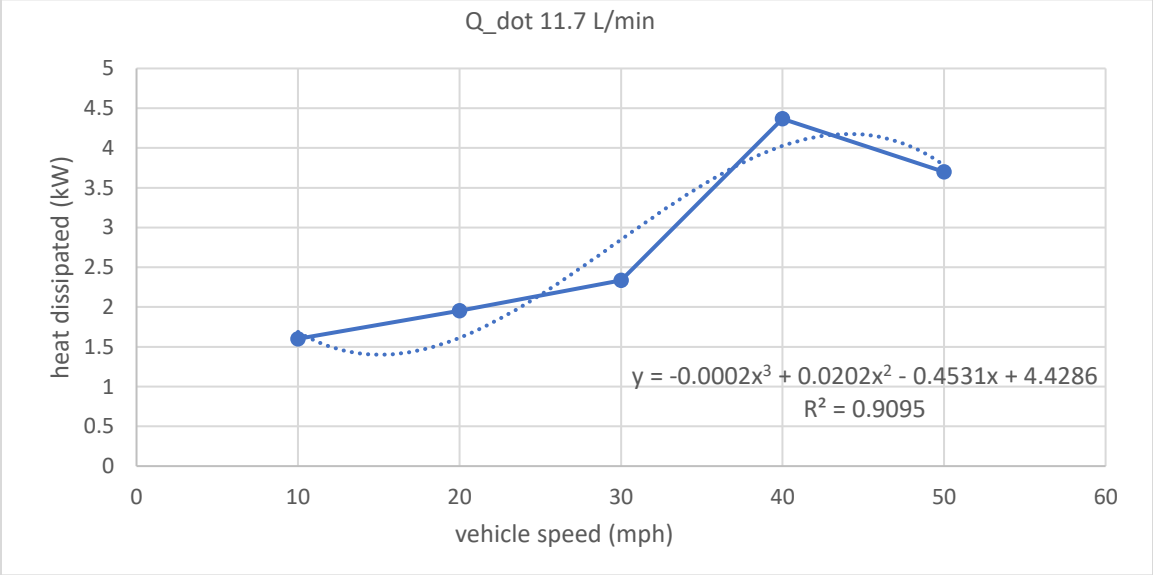

Figure 3 Results of Wind Tunnel Testing at 11.7 L/min

The next set of tests ran was to circulate the water as it was heating to simulate the car starting from idle and running until the temperature reaches steady state. Results from these tests can be seen in figure 4 and figure 5.

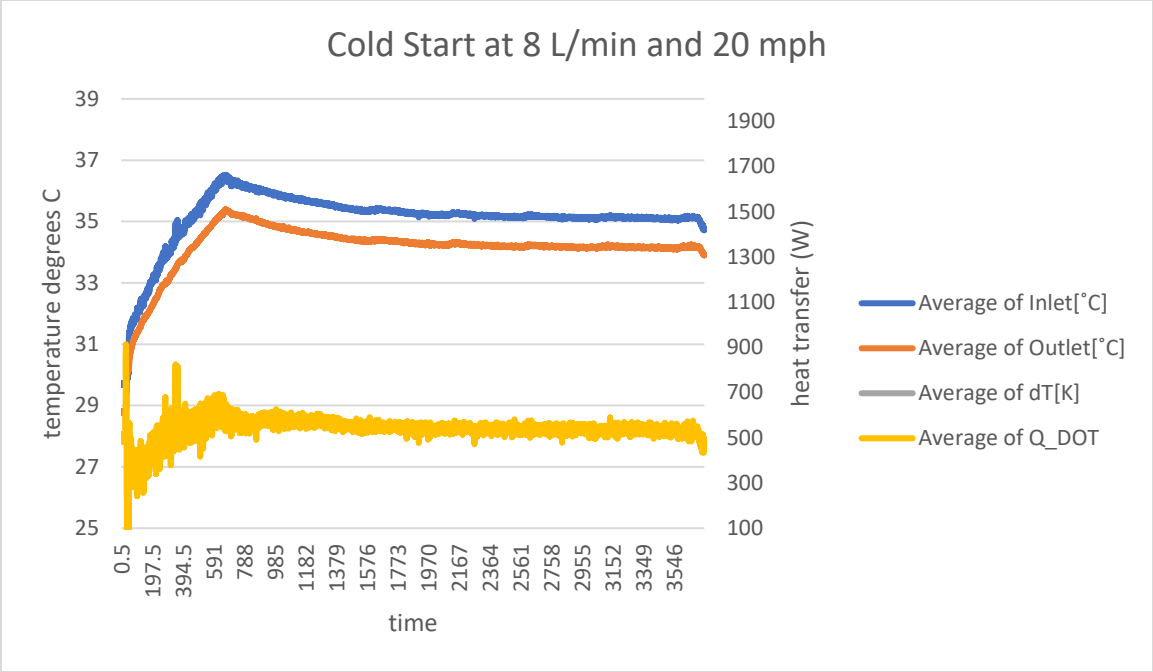

Figure 4 Cold Start test at 20mph

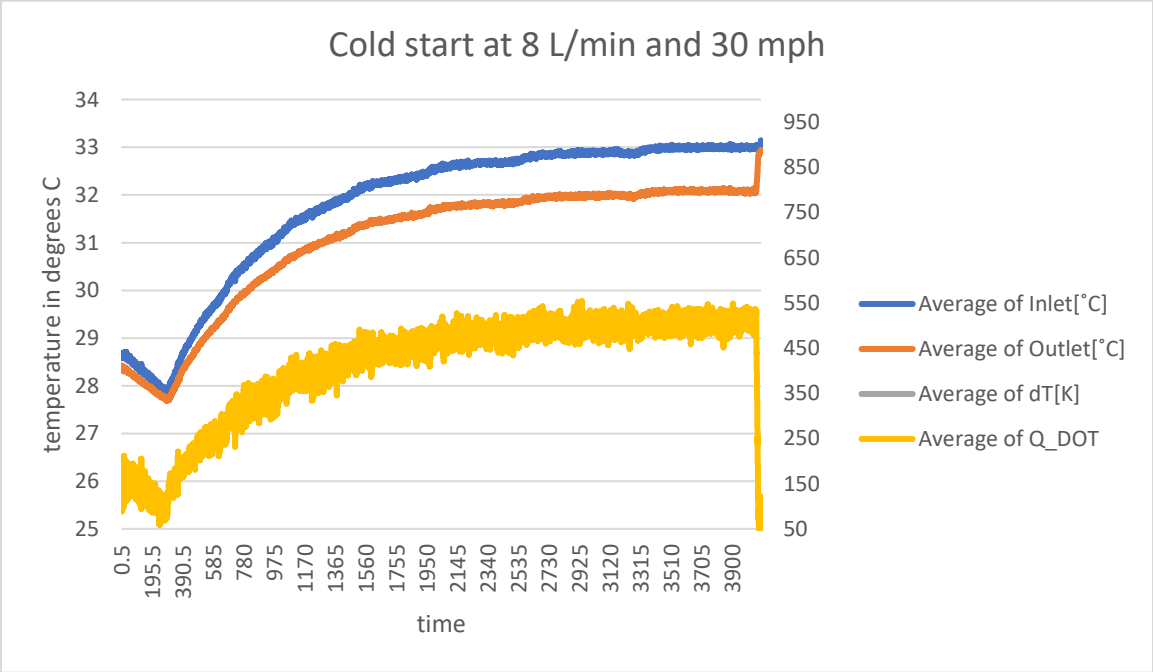

Figure 5 Cold Start Test at 30mph

Steady state data was also collected for routing pre-heated water through the system at wind tunnel airspeeds of 10, 20, 30, 40, and 50 mph. The results, shown in Figure 6, indicates that

there is a decrease in heat lost when velocity is increased from 40 to 50 mph at a radiator angle of 70°.

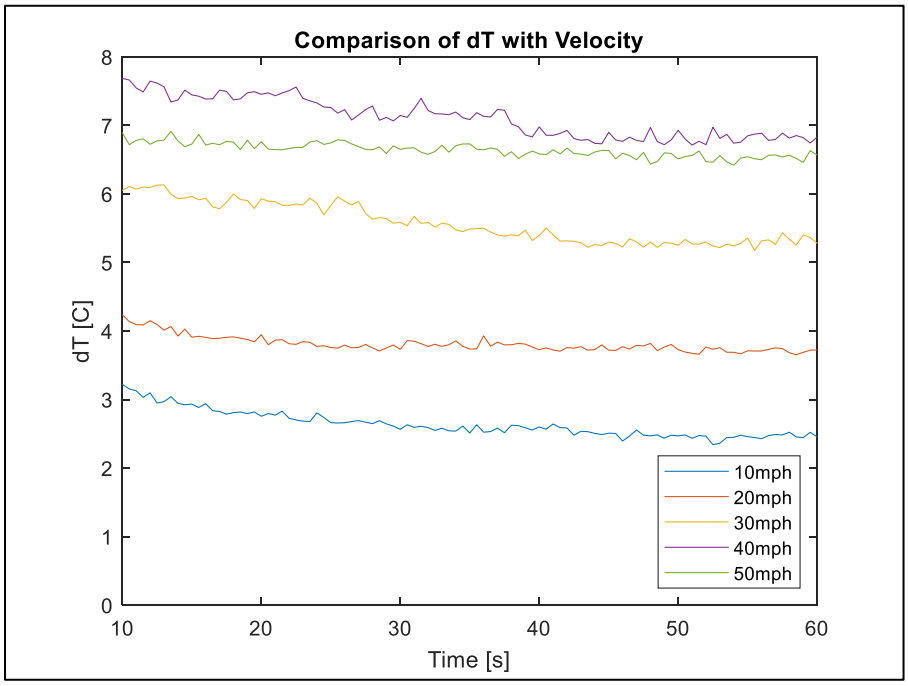

Figure 6. Steady State Heat Dissipation at Given Airspeeds

From all tests performed, the system was able to prove adequacy in maintaining stable and safe operating conditions for longer periods than the ZER 2020 vehicle can operate on a single charge. Although the team's timeslot in the wind tunnel had expired prior to running every test, there was enough information to prove that the design could be effective for the application in which it was to be used.

2.2 Functional Structure Diagrams

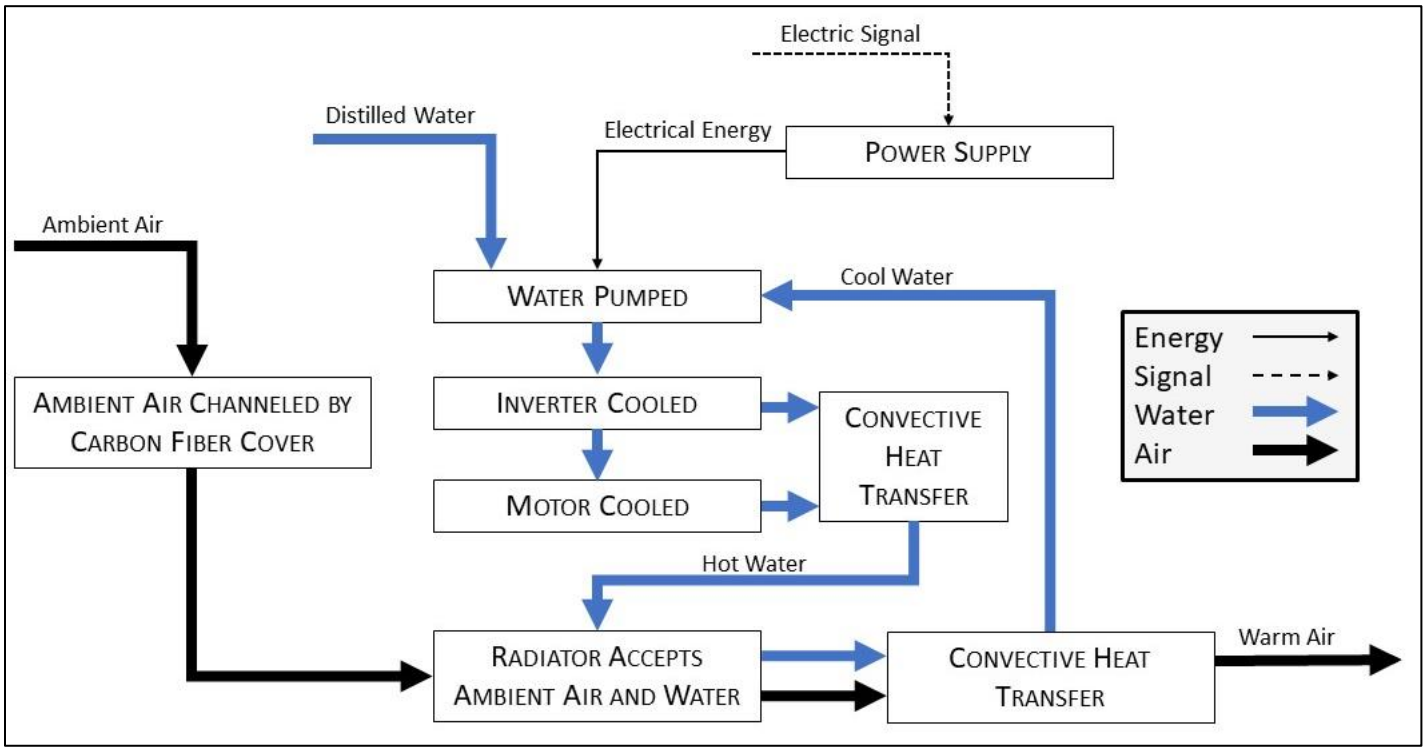

Figure 7. Function Diagram of Cooling System

2.3 Morphological Charts

Table 1. Morphological Chart of Cooling System

Subproblem Concepts				
Maintain structural integrity of chassis	**Channel air onto radiator surface**	**Route all components to avoid other subsystems**	**Reduce flow restrictions**	**Seal system to retain fluid in ±45° tilt test**
Design mount tabs to fail	Fully designed aerodynamic sidepod	*Keep some components outside chassis*	*reduce use of tube joints and limit tube length*	Gimbal system to keep catch can level
Design fasteners to fail	*Simplified side panels*	Keep all components outside chassis	Increase pump size	*Vent cap*
Place radiator inside rollover protection envelope	Forced air (fan system)	Reduce size of components	Increase power supplied to the motor	Fully seal system

The choices made for the final design are italicized in table 1. The choice to design fasteners to fail was the best decision, because in the event of a rollover and the radiator was removed from the vehicle it could be easily replaced by purchasing replacement fasteners. If the

tabs were to fail, then another welding procedure would need to occur before the system could be operational again. The choice to place the radiator inside the rollover protection envelope would be ideal but is not possible due to the space restrictions within the vehicle.

Unfortunately, due to the budget constraints, only a simplified panel cover or forced air fan is possible for the system. The reason for the choice of a simple panel design is not only to simplify CFD analysis models but also to reduce the workload on the vehicle's low voltage system.

Because of the tests ran, it was concluded that the vehicle would not benefit from any of the parts being reduced in size. Because the electric booster pump would be at a risk of damage being outside the chassis, it was decided to only keep the radiator outside of the chassis.

Efficient coolant flow is important in the effectiveness of the coolant system. Because the electric booster pump being used is already near the top of the line in terms of performance and the low voltage system is not able to provide a higher voltage output, it was a simple choice to limit flow restrictions at the source.

Per FSAE rules, the vehicle must be able to withstand a tilt test where it would be subjected to ±45° change in level.in addition, the cooling system must be vented to the atmosphere so that excessive pressure does not build up in the system. For this reason, the only approach was to choose a vent cap that could block flow and allowing pressure to vent. This choice however would not be enough if the vehicle is subjected to a tilt greater than ±45°. However, it is assumed that if the vehicle exceeds ±45° tilt that there will be more significant issues which will take precedence.

2.4 Concept Sketches

The routing of the cooling lines through the radiator (Figure 9), motor (Figure 10), and the inverter (Figure 11) was one of the main factors for the system design. Since flexible tubing was to be used, a simplified concept sketch (Figure 8) was used as the baseline.

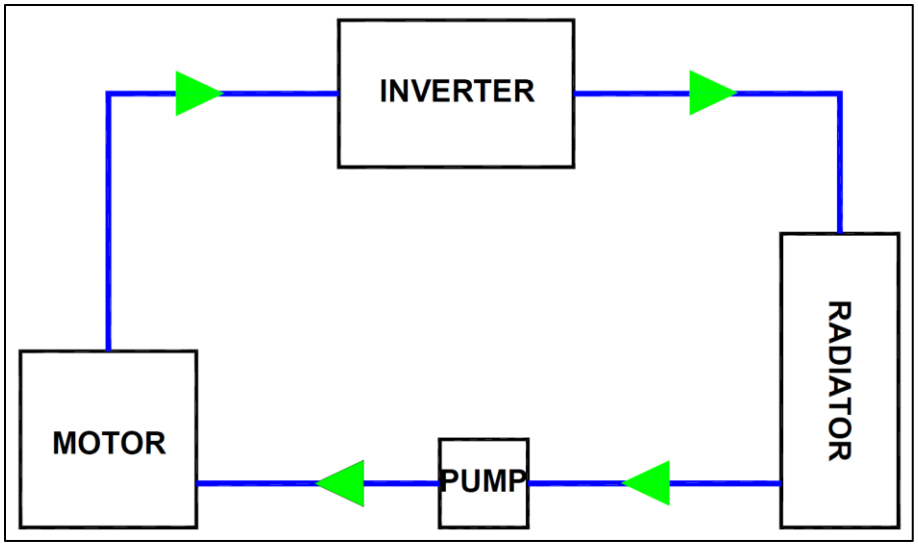

Figure 8. Simplified System Sketch

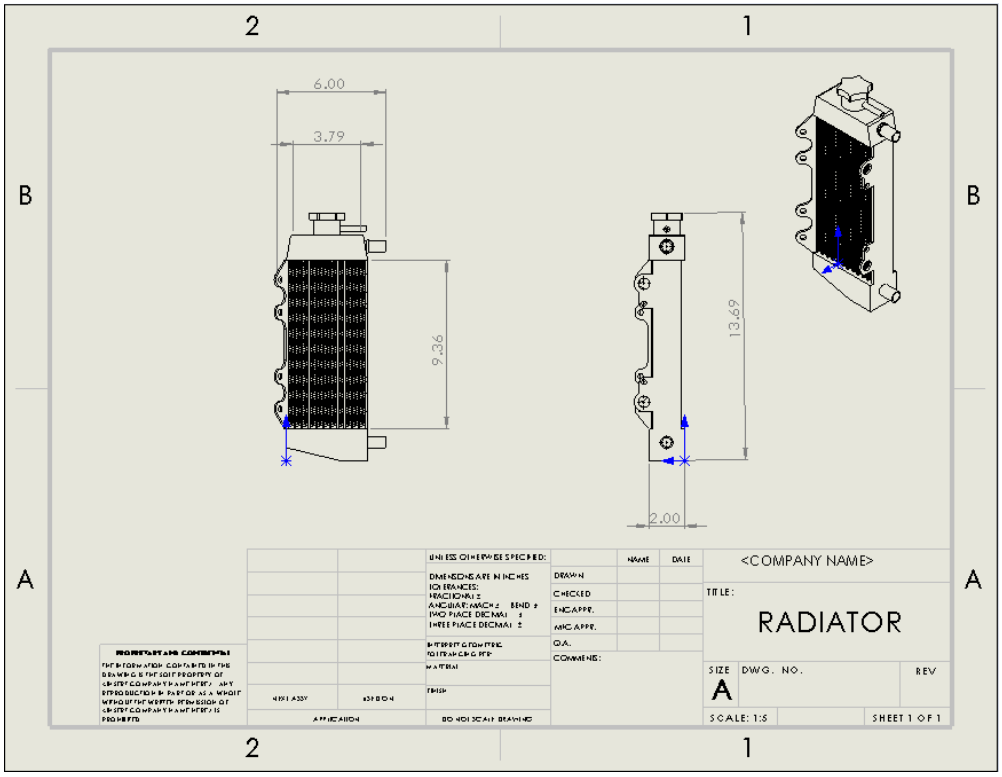

Figure 9. Mishimoto Radiator

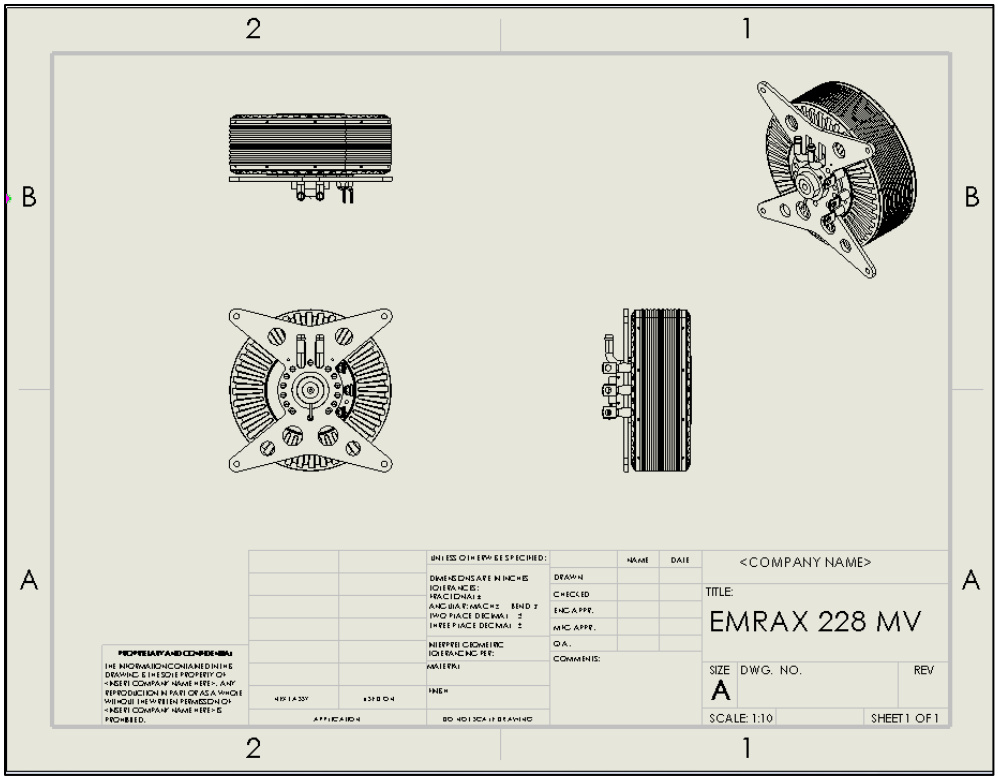

Figure 10. EMRAX® 228 MV

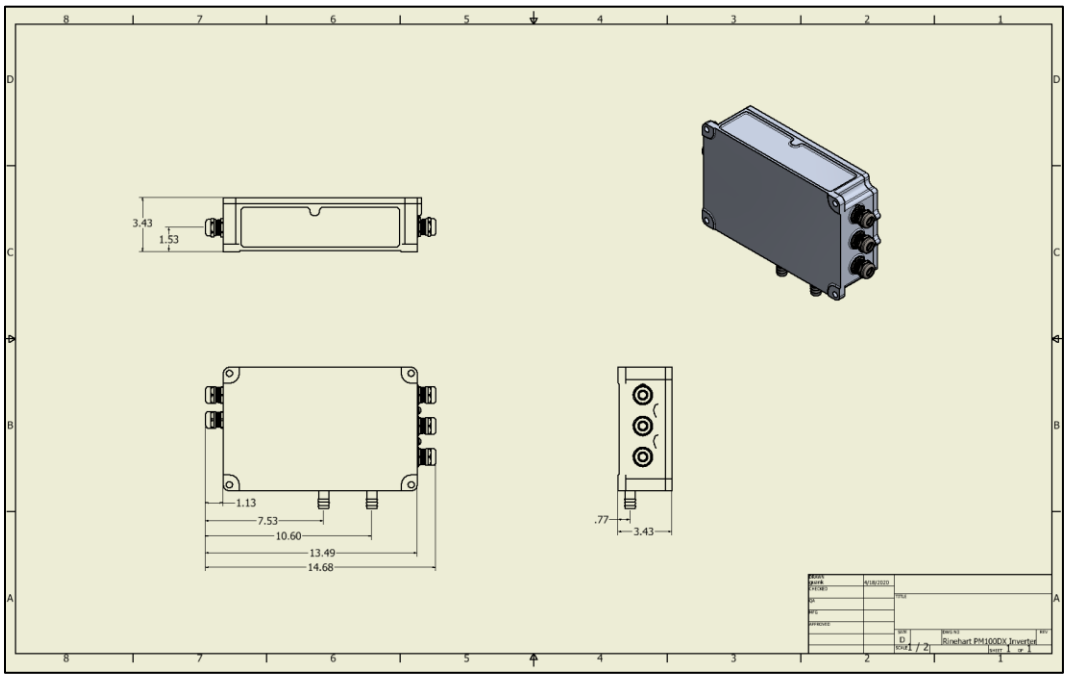

Figure 11. Inverter

2.5 Objective Tree

One tool that can be utilized during the conceptual design stage is a hierarchical objective tree. The objective tree provides a visualization of the importance of each design factor. To represent relative importance, each criterion is assigned a weight with the sum of all weights equaling 1.0. For the cooling system, equal weight was assigned to both the cost and quality of the system. While cost is often sacrificed in formula vehicles for performance, in this instance with tighter budget constraints, it is equally important. Because the materials must be purchased, it is given the highest weight. The manufacturing could potentially be done in house based on the exact design and is therefore given less weight. Repairability of the vehicle is important, but the first goal is to not need to make repairs and put the necessary analysis into the system before building it to ensure that repairs would not be required. For this, repairability is given the lowest weight.

The quality of the system is important for numerous reasons. During the beginning phases of the design it was noted that the entire vehicle was estimated to be overweight by 80lb. This required all subsystems to take part in reducing the weight of the vehicle. However, being that the entire system package was 14.24 lbs. it was important to not add weight to the system. Because the vehicle would not only run for multiple events in multiple races, be transported cross country, and potentially be salvaged for parts in the future, it was equally as important to keep the system operational through these conditions. Lastly, because the time to manufacture the system is long in comparison to the simplicity of the physical system, it was not weighted as highly to stress simplification of the design any further.

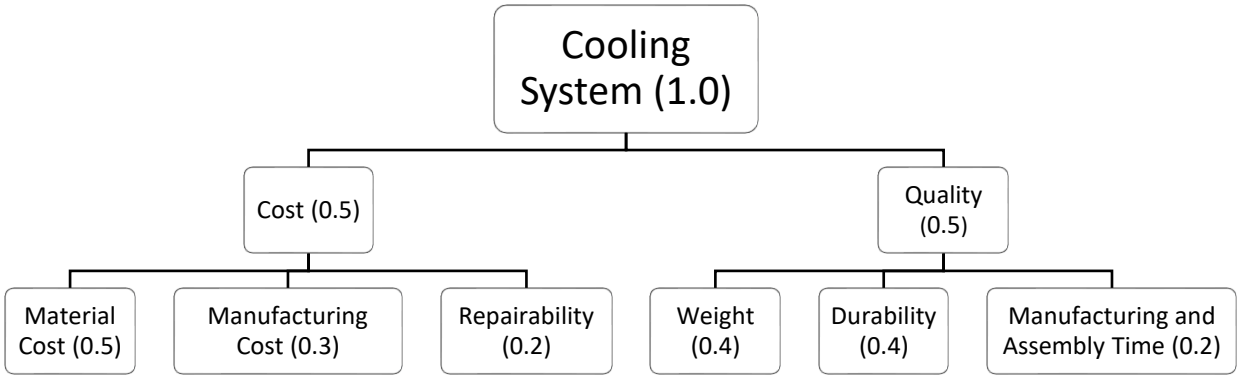

Figure 12 Cooling Subsystem Objective Tree

2.6 Weighted Decision Matrix

Weighted Decision Matrix for Tubing					
		Vinyl (PVC) Tubing		Silicone Tubing	
Design Criterion	**Weight Factor**	**Score**	**Rating**	**Score**	**Rating**
Material Cost	0.5	9	4.5	8	4
Manufacturing Cost	0.3	N/A	-	N/A	-
Reparability	0.2	9	1.8	10	2
Weight	0.4	8	3.2	8	3.2
Durability	0.4	6	2.4	8	3.2
Manufacturing and Assembly Time	0.2	7	1.4	8	1.6
Total			***13.3***		***14***

Figure 13 Weighted Decision Matrix for Tubing Selection

Weighted Decision Matrix for Aero Component							
		Sidepod		Carbon Fiber Cover		3D Printed Ducting	
Design Criterion	**Weight Factor**	**Score**	**Rating**	**Score**	**Rating**	**Score**	**Rating**
Material Cost	0.5	5	2.5	10	5	8	4
Manufacturing Cost	0.3	8	2.4	10	3	10	3
Reparability	0.2	6	1.2	8	1.6	6	1.2
Weight	0.4	9	3.6	10	4	7	2.8
Durability	0.4	9	3.6	9	3.6	7	2.8
Manufacturing and Assembly Time	0.2	5	1	8	1.6	7	1.4
Total			***11.9***		***15.8***		***12.2***

Figure 14 Weighted Decision Matrix for Aero Component Selection

Chapter 3: Embodiment Design

3.1 Schematic Diagram

After selecting the critical components for the cooling system, the simplified system sketch, Figure 8, was updated to show the complete diagram of the system in Figure 15. The only powered component within the cooling subsystem is the Davies and Craig 12V centrifugal pump.

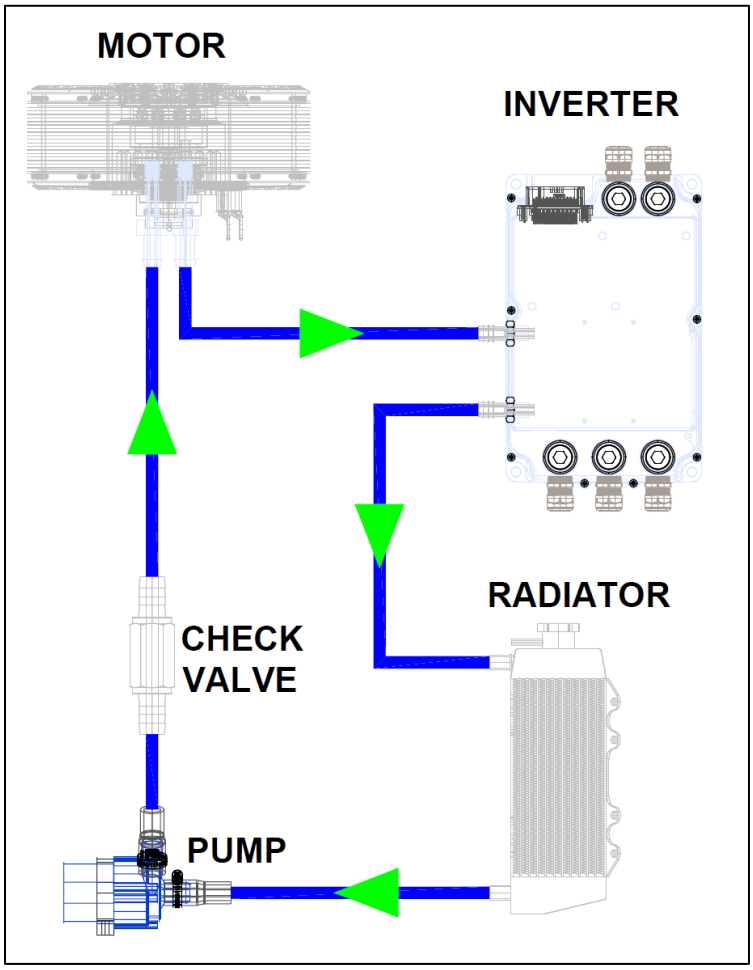

Figure 15. Schematic drawing of essential components

3.2 Configuration Design

Table 2. Material Selections

Component	Material	General dimensions
Radiator	Aluminum	12”x4”x2”
Tubing	Silicone	10’x 0.75”
Hose clamps	Plastic	1”x 0.25”
Side panels	Carbon fiber/ composite	1’x1’x.5”

The choice for the radiator material is limited by the available models on the market. Most products on the market are aluminum because its thermal conductivity of 205 W/m^2K is higher than any other common metal in the same price range.

Silicone tubing was chosen for its cheap cost and its ease of use when installing. Because the designs of the cooling system including other subsystems cannot be expected to be unchanged throughout the design process, the silicone tubing allowed the team to make simple changes to the tube routing to accommodate these changes.

The ideal option would be to use barbed fittings for every interface to limit the number of parts. However, because the motor, inverter, booster pump, and radiator all had different nominal diameters it would require multiple reducers which would increase the number of parts, therefore creating the problem it would seek to solve. The reason for plastic hose clamps is because per FSAE guidelines, all metal components must be electrically grounded. If the team were to choose metal hose clamps, then additional wiring would need to be added running along the entire silicone tubing line to bring all parts to ground. Because many fittings come with a specification of maximum tension, it was possible to find a plastic clamp which did not offer any meaningful sacrifices in strength or weight as compared to metal clamps. Therefore, the simplest decision was to implement plastic material wherever possible.

The side panels were chosen to be carbon fiber because of its light weight. In order to remain compliant with FSAE rules, the carbon fiber panels required a layer of copper within the section to act as a grounding point for the panel. The core of the panel is Nomex composite, a flame-resistant meta-aramid material, which provided a lightweight core to the panel.

3.3 Embodiment Principles

The ZER 2020 team divides the major subsystems into the categories as seen in figure 16. The importance of dividing the systems was to allow team members of different engineering backgrounds to be able to design systems autonomously while keeping a communicational network between teams to be sure that subsystem interfaces would work together once the final assembly began.

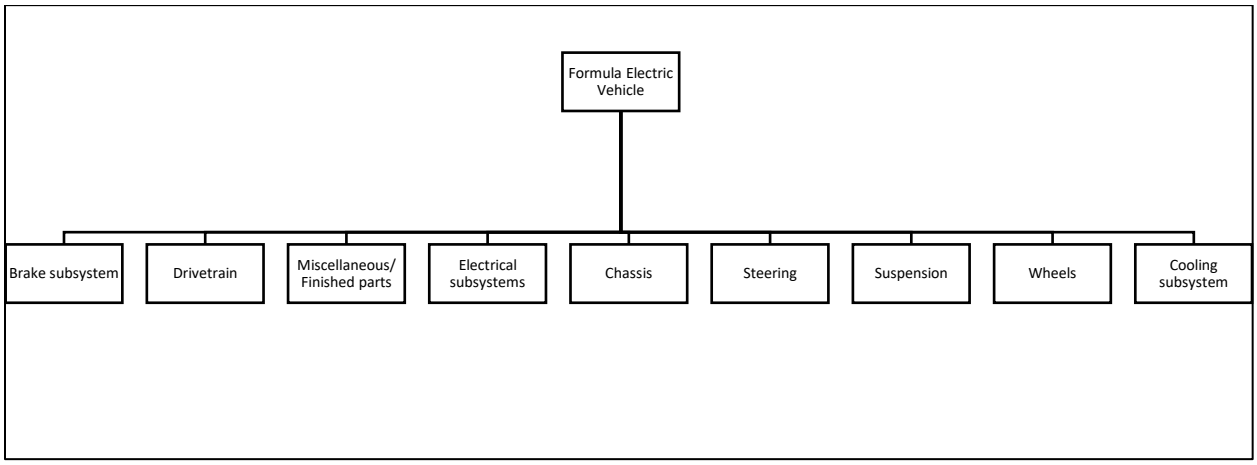

Figure 16. Physical Decomposition of ZER 2020 Vehicle

Most systems are obvious in explanation and interaction within components. The drivetrain and electrical subsystems are heavily intertwined between the electrical and mechanical domains. The chassis, being the frame upon which everything is built is the center of all the subsystems. Therefore, all subsystems must coherently interact with the chassis, specifically in their geometry. Brakes, steering, and suspension teams worked closely together to achieve synergy between the systems. The cooling system is influenced by the electrical and drivetrain systems. The Miscellaneous/ finished parts team would be responsible for projects such as applying aerodynamic top layers to the vehicle body or completing final assemblies on various fasteners.

Figure 17 shows a more elaborate breakdown of the cooling subsystem where the dashed lines represent the interaction of the components. The pump drives the coolant through the tubing to the heat generating systems and then to the radiator. While the system is simple enough to not necessarily need a schematic breakdown, it was found useful for explanations and presentations to teams not working on the cooling subsystem regularly.

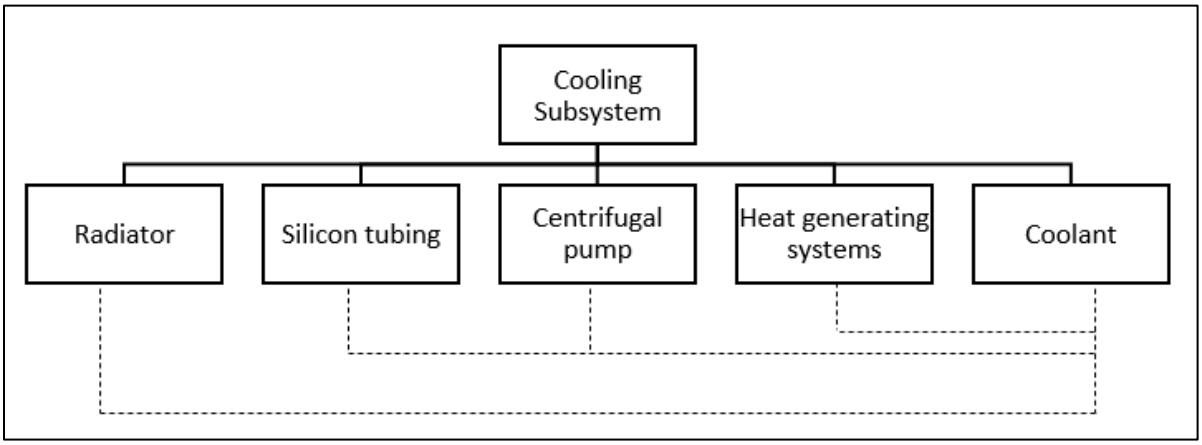

Figure 17. Subsystem Component Expansion

3.4 Failure Mode and Effects Analysis (FMEA)

The purpose of FMEA for the cooling system was to simulate failure of the radiator mounting assemble by applying various forces at predetermined rollover contact points. The criteria being the radiator mounting assembly must fail prior to the chassis in the event of a rollover. The safety factor analysis was chosen to show the assembly interface would fail in multiple simulations. In all simulations, the displacement was magnified for clarity, shown in Figure 18, Figure 19, Figure 20, and Figure 21.

Autodesk Inventor Professional 2019 was used for this analysis. Each simulation was also analyzed to have a magnitude of 1000.0 lb_f applied force. This force was selected to be conservative as the car will never experience a rollover of 1000 lb_f.

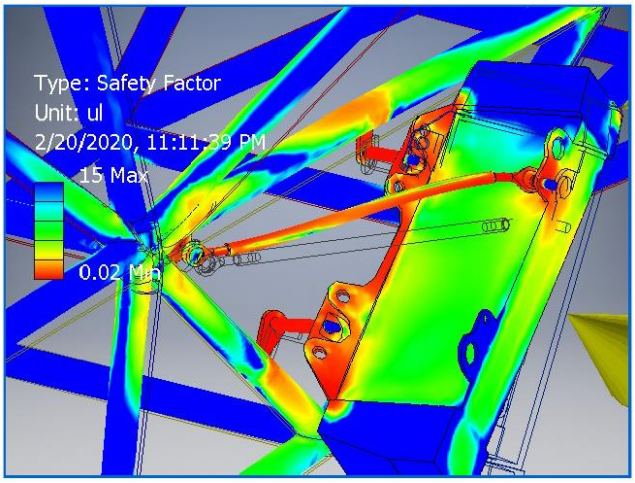

Figure 18. Failure Mode 1 FEA Simulation

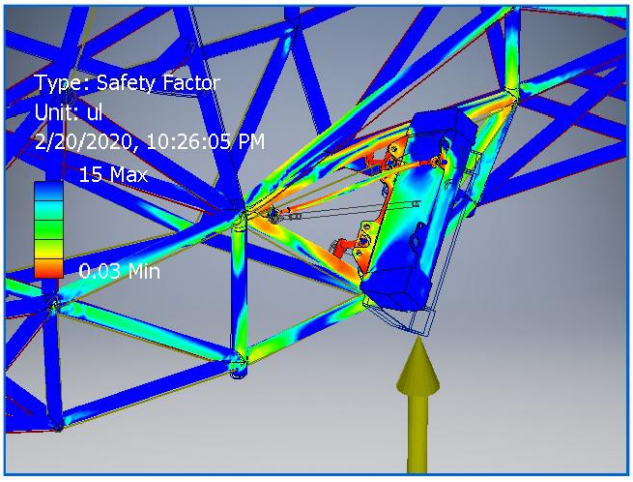

Figure 19. Failure Mode 2 FEA Simulation

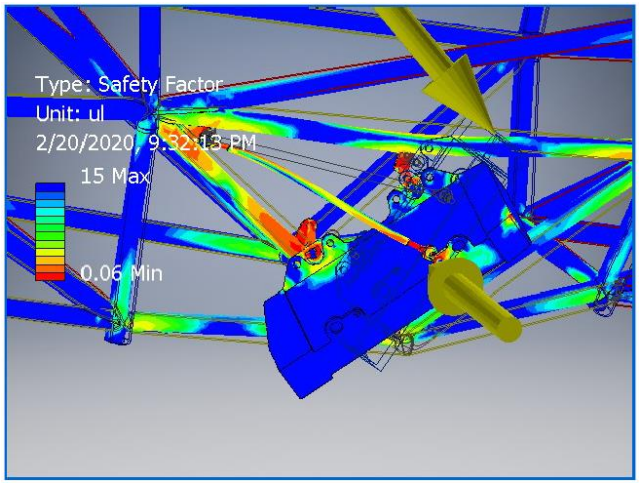

Figure 20. Failure Mode 3 FEA Simulation

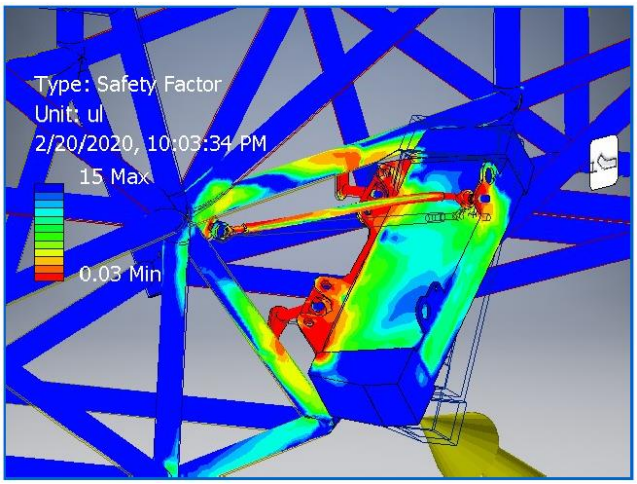

Figure 21. Failure Mode 4 FEA Simulation

3.5 Preliminary Manufacturing Processes

Prior to any parts being assembled or machined, complete part drawings were completed to verify the parts geometry would fit into the allotted space on the vehicle. The assembly drawing can be seen in figure 22, and the manufacturing decisions can be seen in table 3.

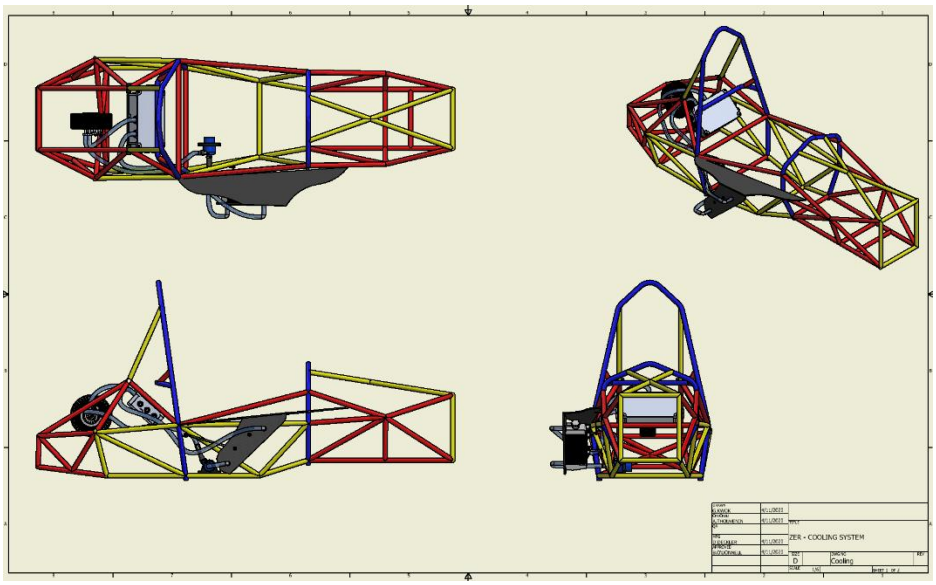

Figure 22. Assembly of Cooling Subsystem

Due to the overall complexity of the vehicle, it was foreseen that there would be design changes apart from the cooling subsystem. The team was able to accommodate all changes from other systems which had forced the cooling subsystem to go through redesign.

Some designs had been removed from the design before the manufacturing phase because of either a cost or a time constraint. Drag reducing sidepods, seen in figure 23, were unable to be manufactured due to the inability to source quality tooling board.

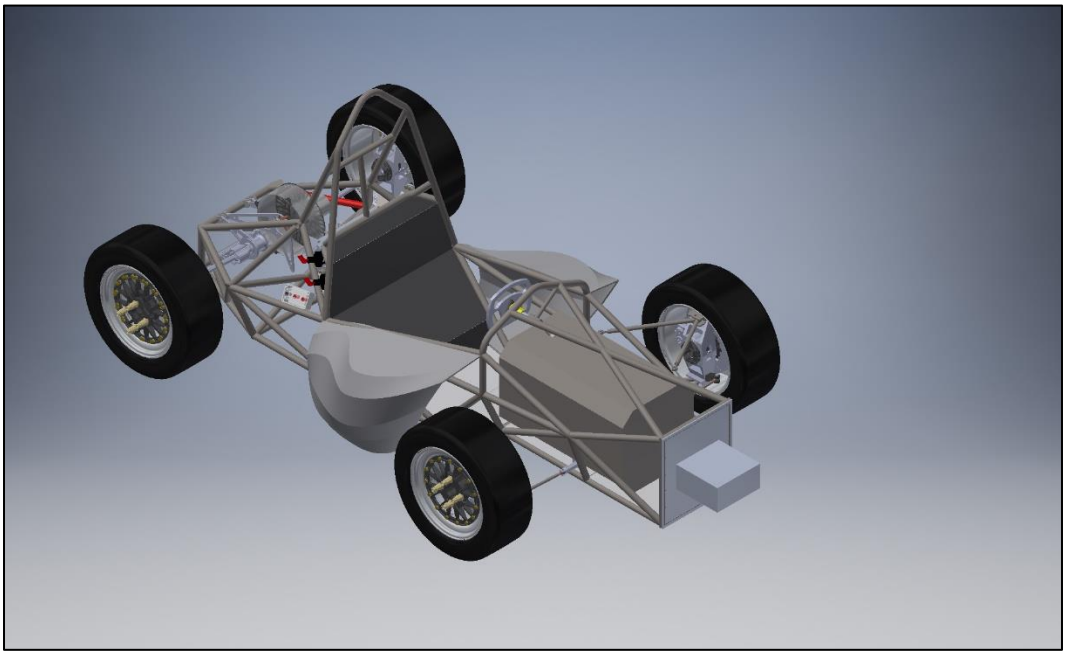

Figure 23. Conceptual Sidepod Design

Table 3 Manufacturing Process for Components

Component	Material	Manufacturing Process
Radiator	Aluminum	N/A
Tubing	Silicone	N/A
Hose clamps	Plastic	N/A
Side panels	Carbon fiber / composite	Hand build
Fasteners	Steel	Lathe
Mounting tabs	Steel	Waterjet
Correction Angle	Aluminum	Mill

The complexity of a radiator makes it unreasonable to manufacture the product in house. The time invested would not outweigh the cost savings and the final product would likely not be of equal quality as from a manufacturer.

The silicone tubing could not be manufactured, but other alternatives were discussed. A carbon fiber prototype tube was built in the first phase of the design project. However, the weight savings of carbon fiber tubes over silicone was, by theoretical calculations, 1.2 lbs. Also, designing a fixture that could allow the rigid carbon fiber tubing to flex during the vibration it would be subjected to present a considerable design challenge. In addition, if any changes were to be made to the system, the entire tubing system would be at risk of being scrapped and redesigned. The extra cost and design time for implementing carbon fiber tubing is significantly higher and if there were to be unforeseen design changes to other subsystems it would require a significant redesign.

The fasteners that were available on the market and originally purchased for the design were, as most things are, built to not fail. However, per FSAE rules it is important that the fasteners do fail as a safety measure against the fasteners causing any deformation to the chassis in the event of a rollover. Because of this design requirement, it was easiest to perform an FMEA simulation on the fasteners and then build mounting rods that met the system requirements.

The manufacturing choice for the mounting tabs was a decision made by the chassis team. All mounting tabs were ordered and manufactured in bulk. The cooling team only had to submit the parts drawings for any unique tabs for the design. Parts drawings for the mounting tabs are in figure 41.

3.6 Wind Tunnel Testing

3.6.1 Background

The Mishimoto radiator supplied by the Zips Electric Race Team had no available technical data sheets (TDS) available to provide the necessary thermal characteristics needed to design a cooling system. To be able to estimate the heat dissipation provided by the radiator, testing was conducted to determine various thermal properties. Testing was conducted at the

AEROLAB Subsonic Wind Tunnel located at The University of Akron. Tests were performed at different forward-facing angles and flowrates to provide sufficient data to extrapolate if needed.

3.6.2 Description

The radiator is approximately 6in x 11in x 2in, made with aluminum, and has 15mm inlet and outlet connector. A 12V Davies Craig centrifugal pump was used. Silicon tubing was used to route the water from an insulated bucket, through the radiator, and back to the bucket. The measured flow rate through least year's system was approximately 7.6 L/min. This flow rate should be similar in this year's car as the components being cooled are identical. The flow rate was controlled with a ball valve and monitored with a flow meter. Temperature readings were initially recorded at one second intervals by hand before a data acquisition system was provided by Collins Aerospace.

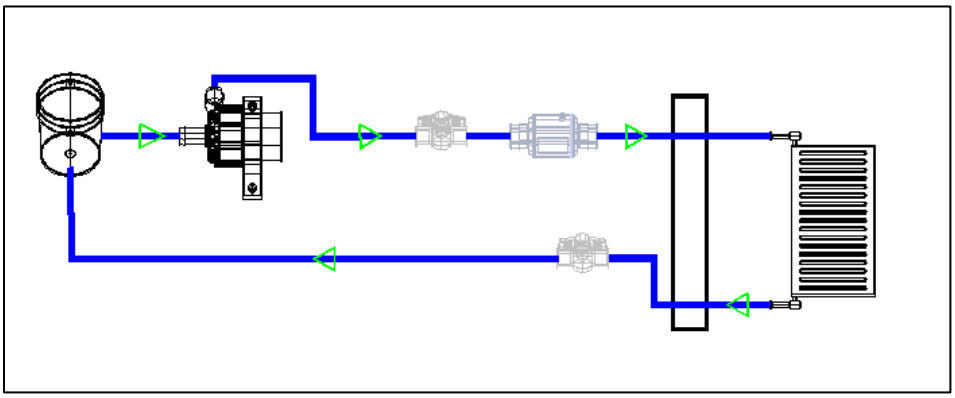

Figure 24. Schematic of System Tested in Wind Tunnel

3.6.3 Test Facility

A radiator mounting fixture, Figure 25, was fabricated to be adjustable to simulate different radiator mounting angles. A 3D model of the wind tunnel test section, Figure 26, was used to check for interferences and confirm placement of the full assembly.

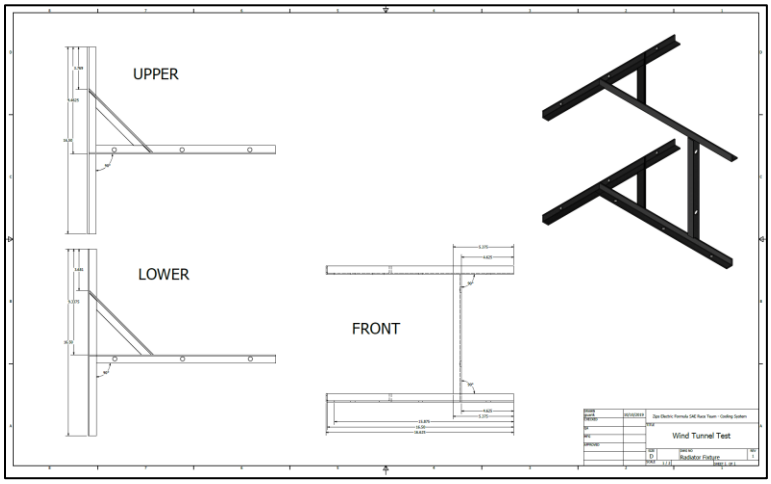

Figure 25. Wind Tunnel Test Fixture

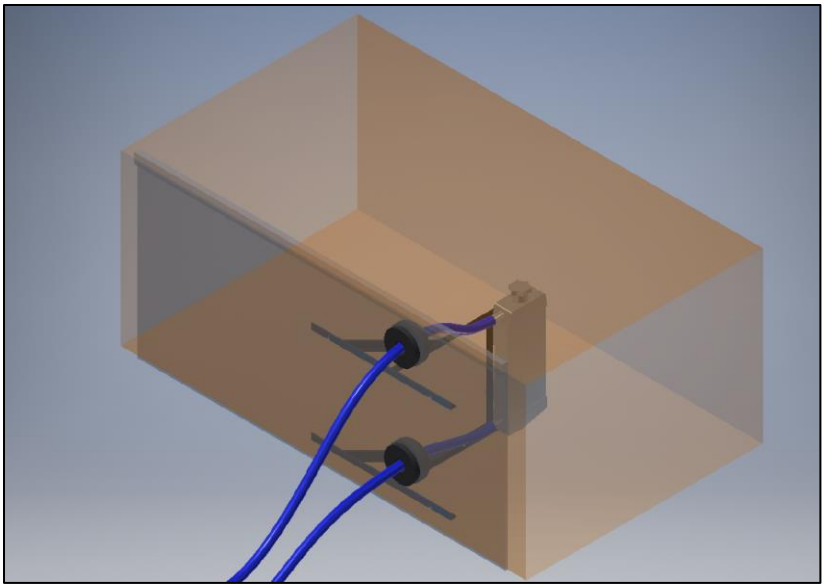

Figure 26. 3D Model of Wind Tunnel Test Environment

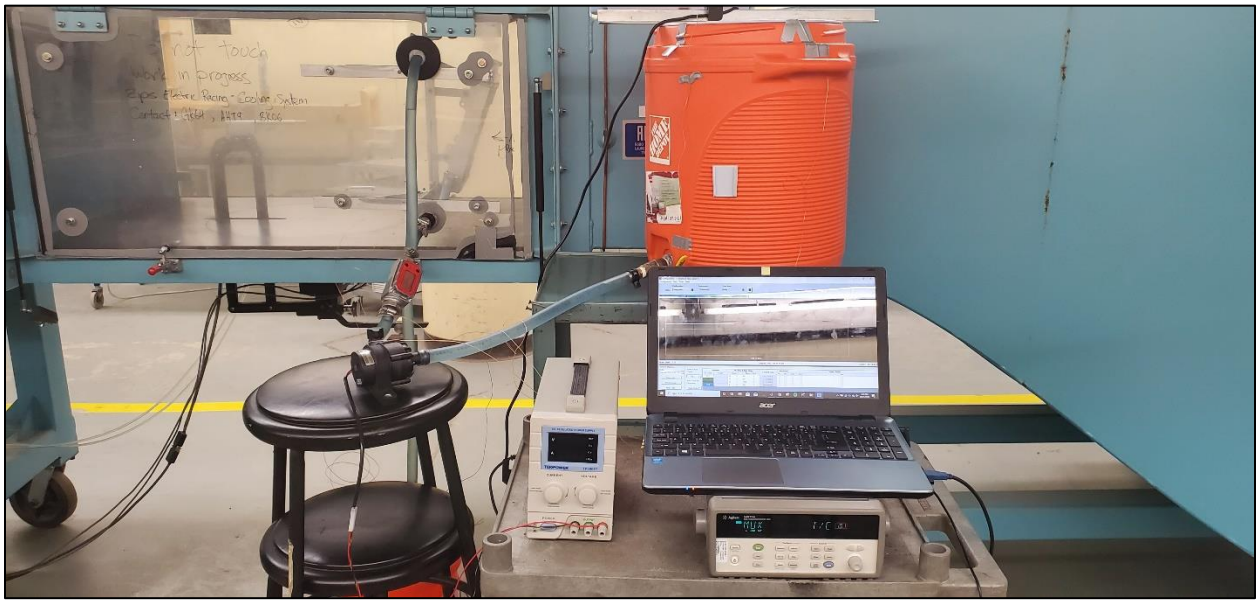

Figure 27. Test Equipment and Setup for Wind Tunnel Testing

Figure 28. Vertically (90°) Mounted Radiator

Figure 29. Angled (70°) Mounted Radiator

3.6.4 Data

The data acquisition system (DAQ) used was an Agilent 34970A series, courtesy of Collins Aerospace. The system took measurements once per second. The data from the acquisition system exported the numerical values as Excel .csv (comma-separated values) files. From there the data collected was analyzed with both Microsoft Excel and MATLAB using calculations outlined in section 3.7. The results showed that the system designed was effective at dissipating enough heat to allow the vehicle to remain operational. An example of the data exported to Excel is shown in figure 30. The centrifugal pump voltage and current was also recorded by the system as the wind tunnel test was performed early in the design process. However, the ability to vary the voltage was discarded early as the low voltage system could not accommodate a variable voltage source.

Scan	Time	%Time(s)	%Ambient(F)	%RadSurface(F)	%Inlet(F)	%Outlet(F)
1	10/21/2019 19:38:48:196	0	75.991	76.136	158.704	77.357
2	10/21/2019 19:38:48:692	0.5	75.996	76.171	158.857	77.364
3	10/21/2019 19:38:49:192	1	75.983	76.154	158.749	77.351
4	10/21/2019 19:38:49:692	1.5	75.955	76.149	158.728	77.341
5	10/21/2019 19:38:50:192	2	76.019	76.149	159.102	77.287
6	10/21/2019 19:38:50:692	2.5	76.007	76.189	158.823	77.317
7	10/21/2019 19:38:51:192	3	76.03	76.171	158.863	77.263
8	10/21/2019 19:38:51:692	3.5	76.037	76.142	158.983	77.305
9	10/21/2019 19:38:52:192	4	76.037	76.16	158.789	77.294
10	10/21/2019 19:38:52:692	4.5	76.072	76.217	158.897	77.333

Figure 30. Data Acquisition Output

3.7 Numerical Calculations

The cooling systems design and fabrication was verified through analytical calculations to ensure that the system could meet the design parameters. The system components contributing to heat added to the system are in Table 4.The free body diagram, Figure 31, along with Table 4 was used to derive the necessary equations to evaluate the thermal characteristics of the system.

Table 4 Heat Generating Systems

	Max power	Efficiency	Heat Dissipated (Max)
Motor	60kW	90%	6kW
Inverter	80kW	97%	2.4kW
Pump	24W	Assumed 100%	Negligible

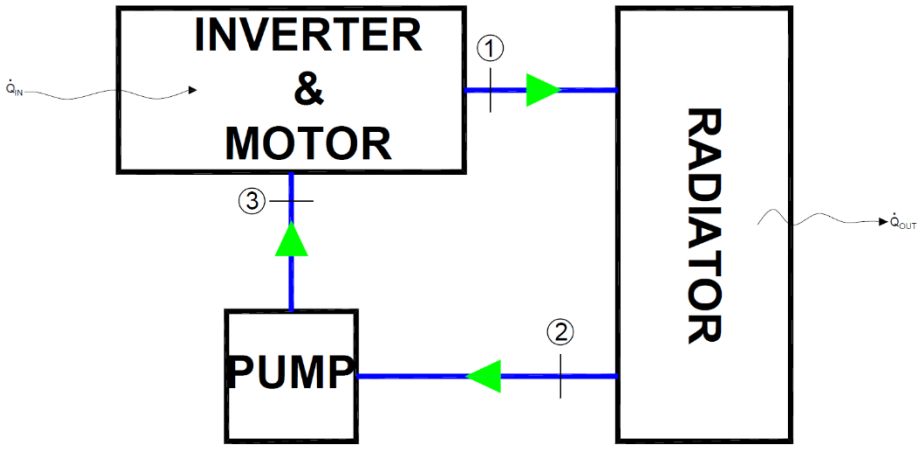

Figure 31. Free Body Diagram

Because the centrifugal pump is, by comparison, insignificant in its contribution to the heat generated, it is considered an ideal pump with no losses.

The equation for the surface heat transfer of a finned radiator:

$$A_{rad} = \frac{\dot{Q}}{(T_{rad} - T_{\infty}) * h_{\infty}} \quad (3.1)$$

Where A_{rad} is the area of the radiator, $\dot{Q}$ is the rate of heat transfer out of the system, T_{rad} is the temperature of the radiator surface, T_{∞} is the temperature of the surroundings, and h convective heat transfer coefficient of the ambient surroundings.

The mass flow rate through the system is important to know to establish how much coolant is entering the radiator during any period of time.

$$\dot{m} = \rho_{water} * V_{sys} * A_{sys} = Q_{sys} * \rho_{water} \quad (3.2)$$

Where $\dot{m}$ is the mass flowrate, V is the velocity, and Q is the volumetric flowrate. Solving equation 3.2 where $Q_{sys} = 7.4 \frac{L}{min} = 0.0001233 \frac{m^3}{s}$:

$$\dot{m} = 0.000123 \frac{m^3}{s} * 1000 \frac{kg}{m^3} = 0.123 \frac{kg}{s}$$

The maximum amount of heat dissipated by the system can be found by the following

$$Q_{out} = \dot{m} * c_P * (T - T_{\infty}) \quad (3.3)$$

Where Q is the energy out, and c_p is the specific heat. Resulting in

$$\dot{Q}_{out} = 0.123 \frac{kg}{s} * 4.13 \frac{kJ}{kg * K} * (65 - 27) = 19.3036kW$$

For a realistic system, solving equation 3.1 for T_{rad}, becomes

$$T_{rad} = \frac{\dot{m} * C_P}{\dot{Q}_{out}} + T_{\infty} \quad (3.4)$$

Therefore, the temperature the system would reach would be

$$T_{rad} = \frac{0.123 \frac{kg}{s} * 4.13 \frac{kJ}{kg * K}}{9kW} + 27 = 44.72°C = 112.5°F$$

3.7.1 Weight Calculations

Table 5. Model Properties of Radiator

Mass Properties of Radiator	Value	Units
Density	0.10	lb_m/in^3
Mass	4.65	lb_m
Volume	2108.48	in^3
Surface Area	2108.48	in^2

Table 6. System Weight by Part

Component	Value	Units
Radiator	4.65	lb_m
Silicone Tubing	1.6lb	lb_m
Carbon fiber Tubing	0.4*	lb_m
Coolant water	2.31	lb_m
Centrifugal pump	2	lb_m
Catch can (empty)	1.2	lb_m
Side panel	2.48	lb_m
Total System Weight	14.24	lb_m

** Theoretical value, part not implemented into system*

Chapter 4: Detail Design

4.1 Finite Element Analysis (FEA)

The FEA simulations were run in parallel with the FMEA safety factor simulations outlined in the previous FMEA section. The FEA simulations were also ran in Autodesk Inventor Professional 2019 to determine the Von Mises Stresses of radiator mounting assembly. These simulations were not required to meet the FSAE requirements. However, the Von Mises Stresses further show that the stresses endured by the mounts will cause failure prior to the chassis. The displacement of the components are again magnified for clarity.

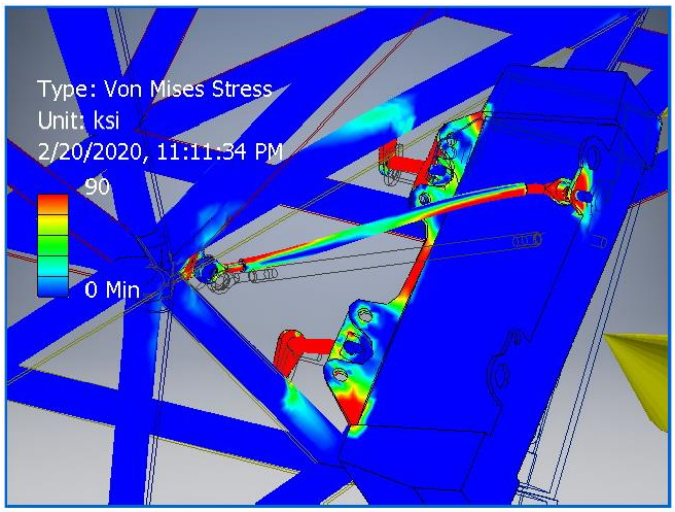

Figure 32. Force Mode 1 of FEA Simulation

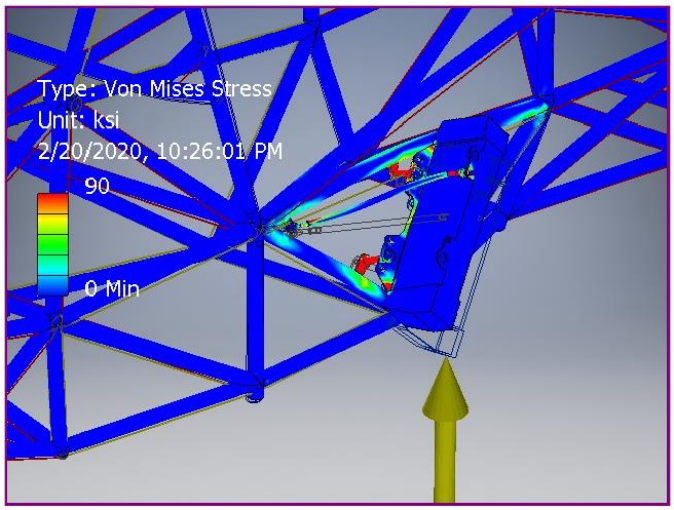

Figure 33. Force Mode 2 of FEA Simulation

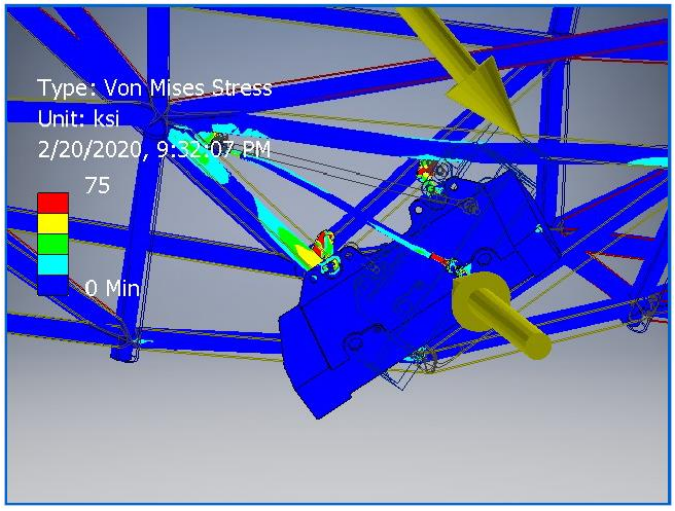

Figure 34. Force Mode 3 of FEA Simulation

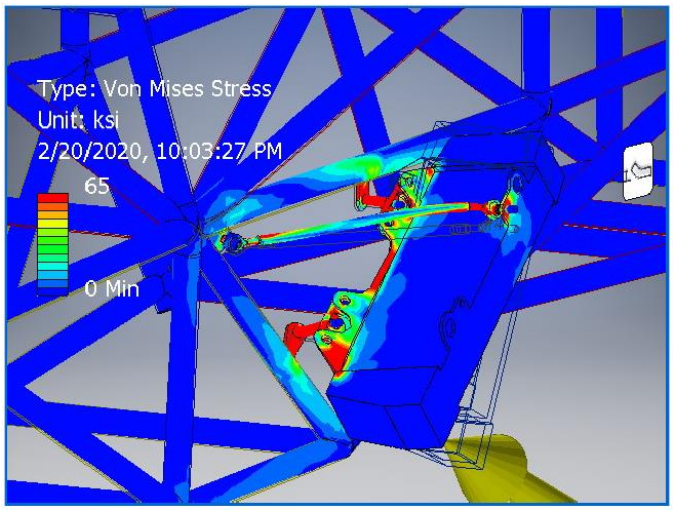

Figure 35. Force Mode 4 of FEA Simulation

4.2 Computational Fluid Dynamics (CFD)

In consideration of the team budget limitations, a panel style radiator cover was designed and tested in the CFD model. The panel allows the airflow to be channeled into the radiator as well as protect the radiator from debris that may impact the fins of the radiator during a race. Because of the budget constraints from ZER 2020 there is room for improvement on the sidepod cover to not only increase the cooling effects, but also reduce the aerodynamic drag.

The student version of ANSYS Fluent CFD allows a limited number of mesh nodes (525000). For this reason, the model had a wrap applied to it in order to reduce the necessary mesh nodes to converge onto a solution. Unfortunately, without a different license version of Ansys it is not possible to improve the results from here.

The program itself can be used again for future vehicles as well. Because the setup of the program is complete, it is only necessary to upload a new geometry and re-mesh the assembly and run the program to analyze again. Velocity was increased in all CFD simulations for better visualization of the flow.

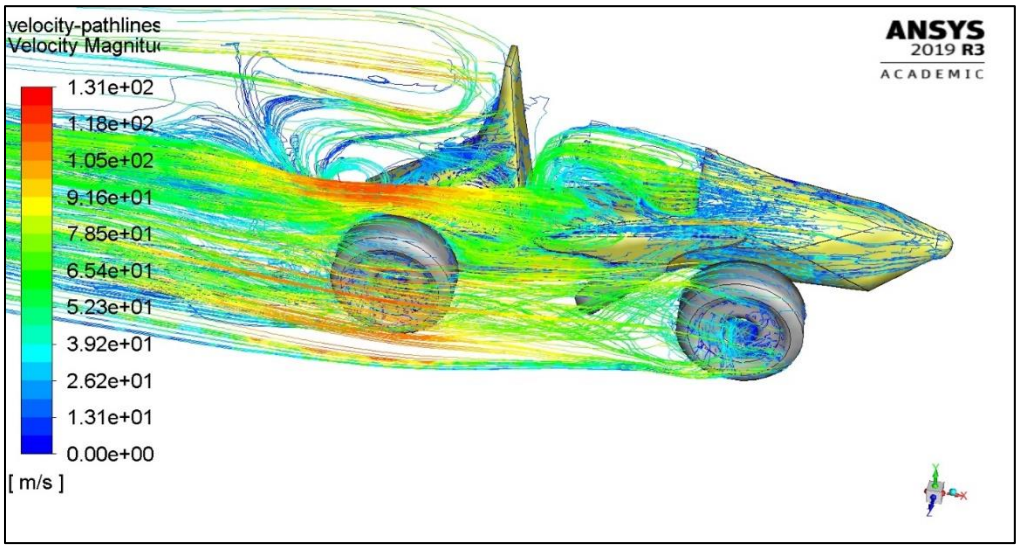

Figure 36. CFD Model with Streamlines

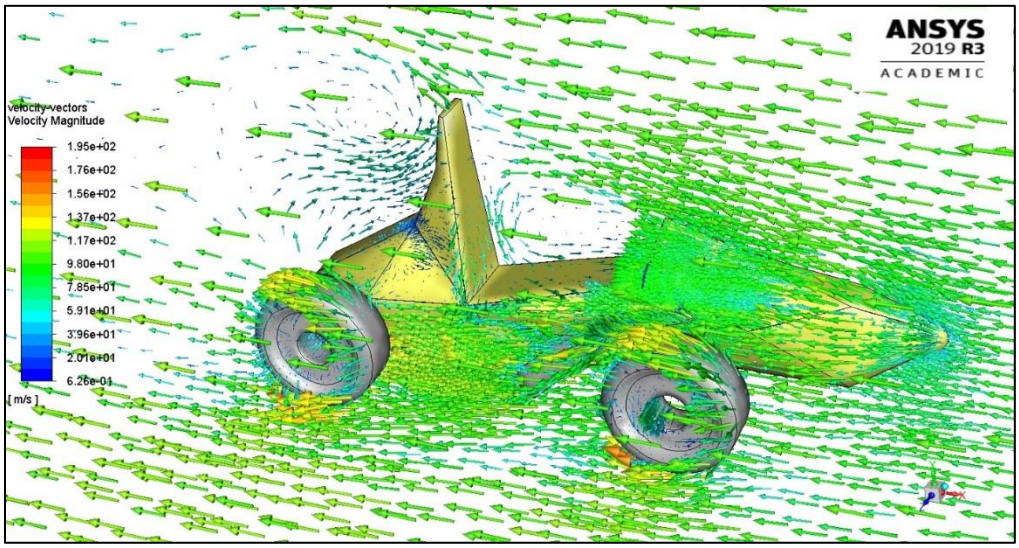

Figure 37. CFD Model with Velocity Vectors

4.3 Simulink Model

In order to create a baseline simulation of the cooling system, a Simulink model was created using the thermal modeling add-on. The effort is to alleviate the need for wind tunnel testing by the cooling team in the future. The system is simplified to calculate one convective heat source into the system and one convective heat source out of the system. This model runs in

a closed loop configuration but can easily be changed to an open loop configuration by breaking the connection and adding another reservoir.

While this model provides an excellent baseline for modeling a thermal system, there are some drawbacks to the model. Firstly, all the heat transfer coefficients are lumped into two convective sources which does not allow the thermal properties of the air, water, and aluminum to modified separately. Secondly, this model uses a simple thermal liquid to thermal control heat exchanger. For proper modeling of the airflow, a thermal liquid to gas system heat exchanger should be employed to allow the model to analyze various air speeds. Lastly, the model uses a constant displacement pump to eliminate reverse engineering of the centrifugal pump's parameters. If the system is to be most accurately model though, the pump should be properly modeled in the system.

Some parameters of the system, such as the radiator surface area and heat transfer coefficients of simple materials like aluminum and copper, is well known other parameters such as the exact heat taken away by the air and the exact amount of power that enters the coolant water is not so well known. While the exact power dissipated by the motor and inverter is known, because both systems are housed in thermally conductive housings it is unknown exactly how much of the heat is transferred by convection directly away from the systems from the housing surfaces. For this reason, the model was designed with an iterative process to attempt to match these unknown values to the observed tests.

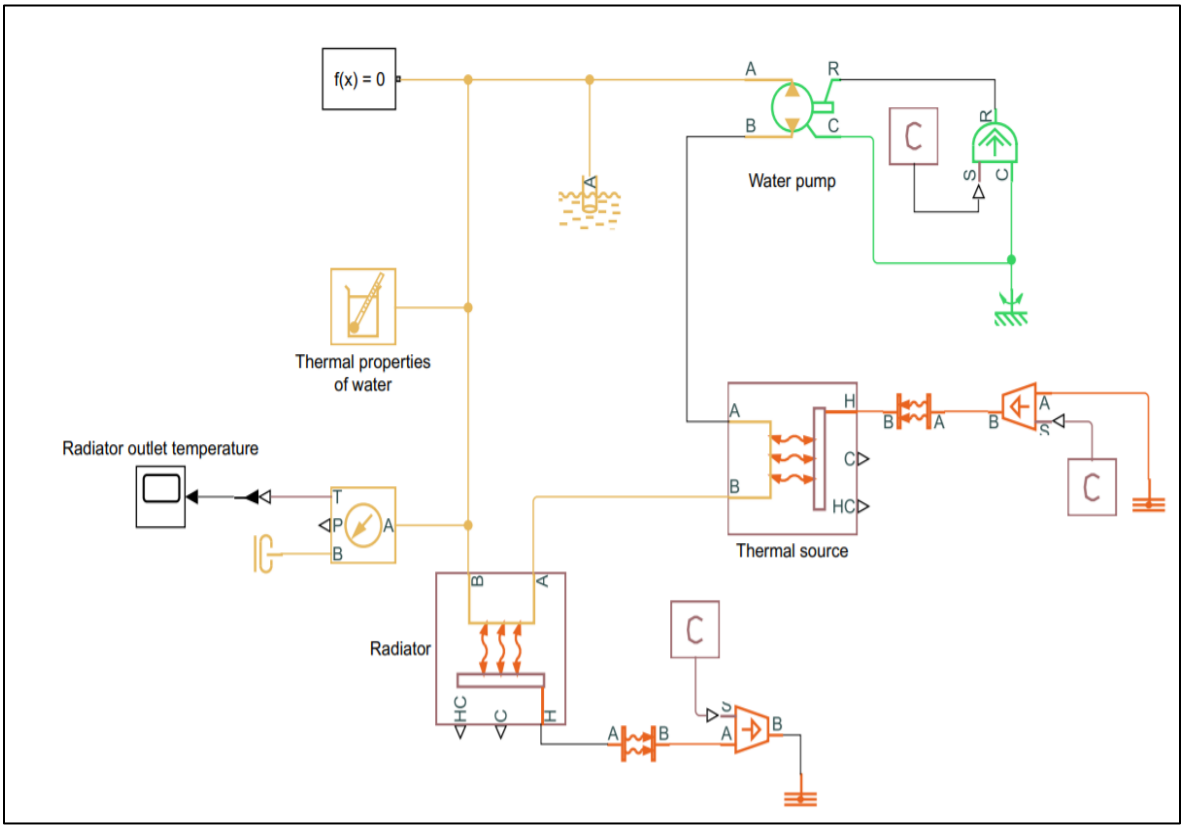

Figure 38. Simulink Model

The results of the Simulink model can be seen in figure 39. As is the case with most thermal systems, the results of the model appear to be an overdamped first order model. The solver configuration uses MATLAB's built in ode23 function to converge on a solution. Because this model can be represented by a first order differential algebraic equation, the choice to use the ode23 function is appropriate. From the results, the final steady state outlet temperature is 35°C which is in line with the output results of the wind tunnel test.

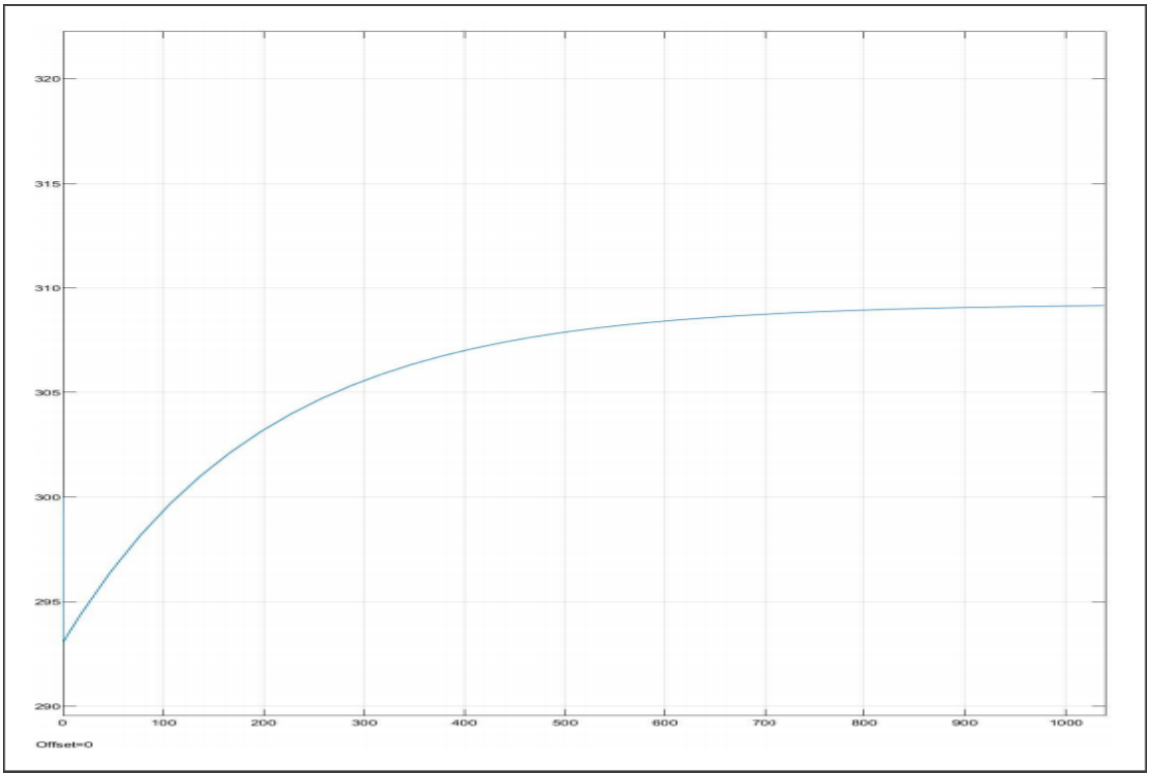

Figure 39. Simulink Model Results

4.4 Component Selection

For all the testing performed, the parts used were purchased by ZER 2019 cooling team. Because of budget constraints for the team, parts were unable to be purchased until a system had been fully designed to eliminate unnecessary purchases. In order to establish a performance baseline, the parts purchased were fully tested using the wind tunnel test described in section 3.7.

After necessary tests concluded on the selected parts, it was determined that due to the thermal efficiency of the system it would not be necessary to purchase new components. There is the potential for weight savings by purchasing different system components, but for the order of 1-5 lbs. it was deemed unworthy of the expense.

The centrifugal pump was also well suited for the task since it is the lightest pump on the market which can handle a continuous 8L/min output in the system as well as operate on 12VDC which meets the requirements of the low voltage system of the vehicle. All the connection lines to the centrifugal pump and radiator are silicone, again because it is a cost friendly and easy to

work with and route through the tight spaces. The coolant water was restricted because the inverter specifically requests distilled water be used as the only coolant.

The mounting tabs were designed to accommodate the shape of the chassis and were cut from the same steel as from which the chassis is made so that they could be welded to the chassis. The fasteners to the radiator were machined to be FSAE rules compliant and deform before causing damage to the chassis in the event of a rollover. Drawings for the fasteners cans be seen in Figure 41.

4.5 Part Drawings

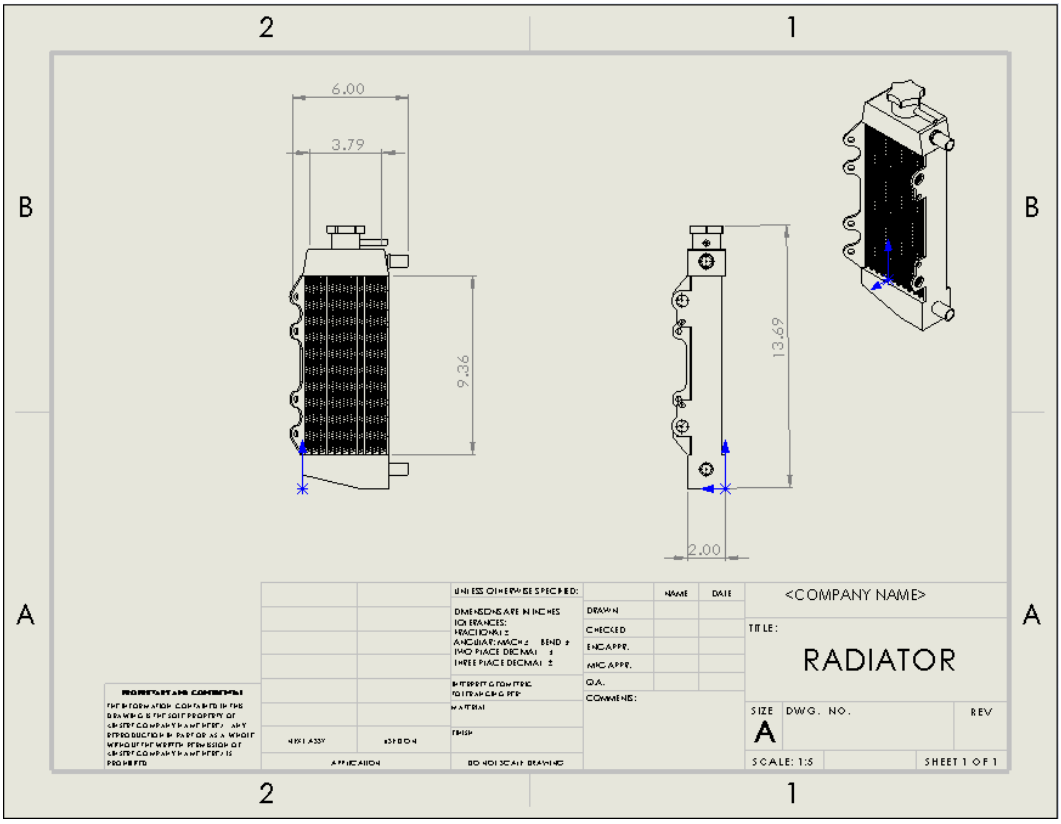

Figure 40. Radiator Part Drawing

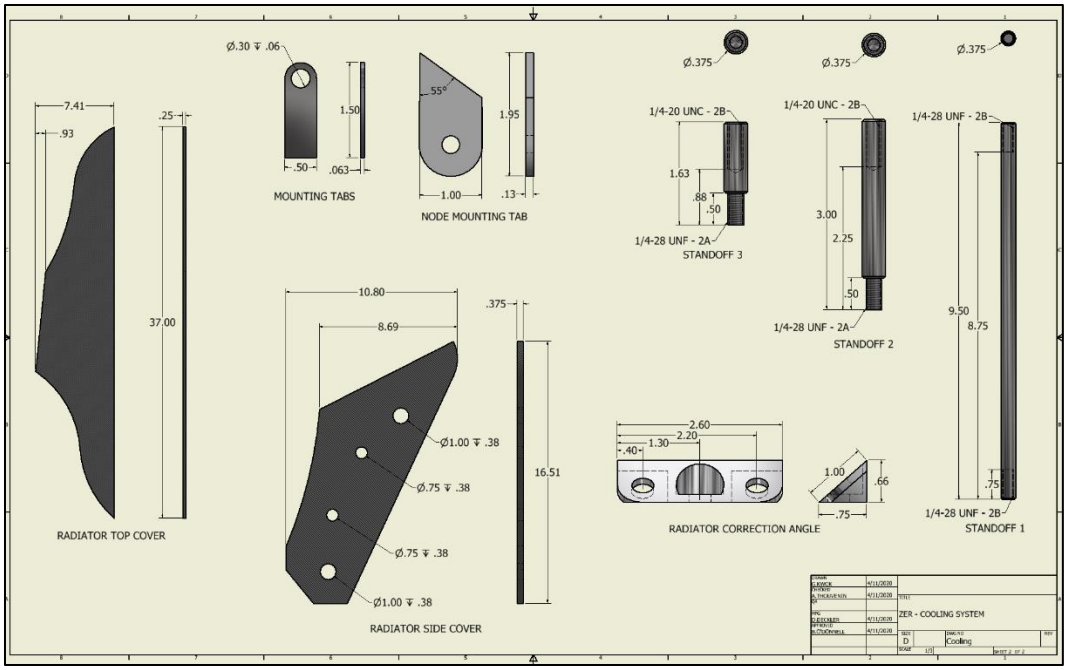

Figure 41. Radiator Panel and Fastener Part Drawings

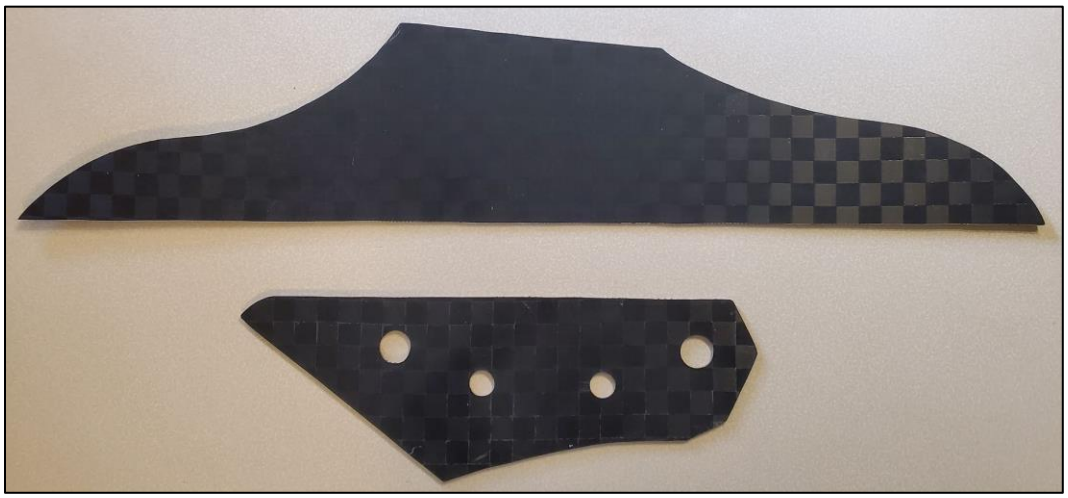

Figure 42. Finished Prototype: Radiator Panels

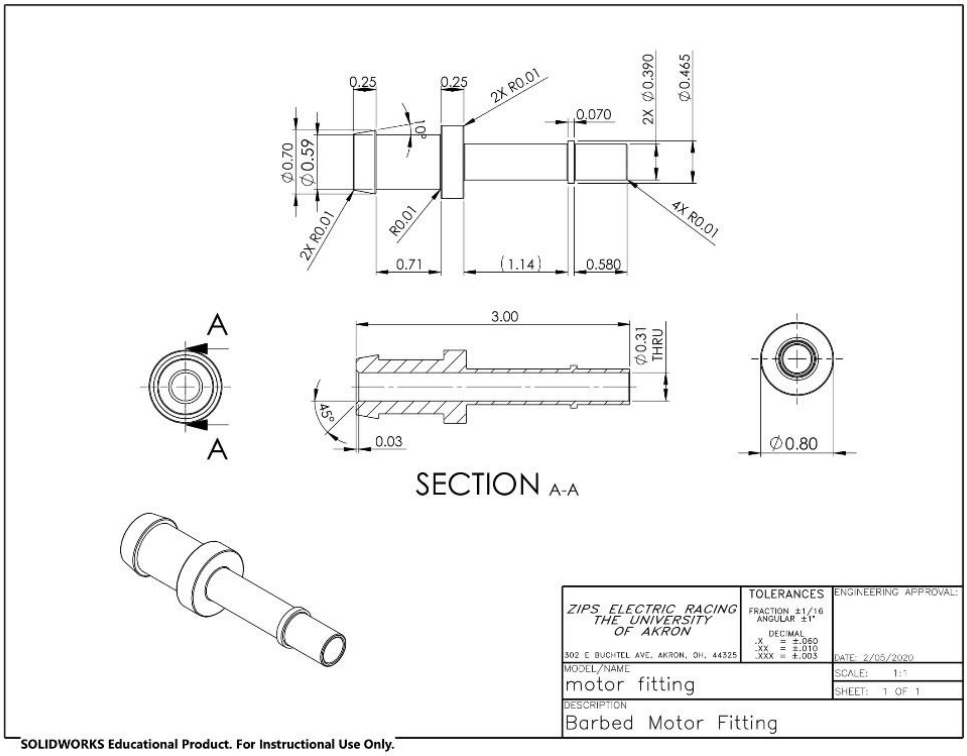

Figure 43. EMRAX® Motor Adapter Fitting

4.6 Assembly Drawings

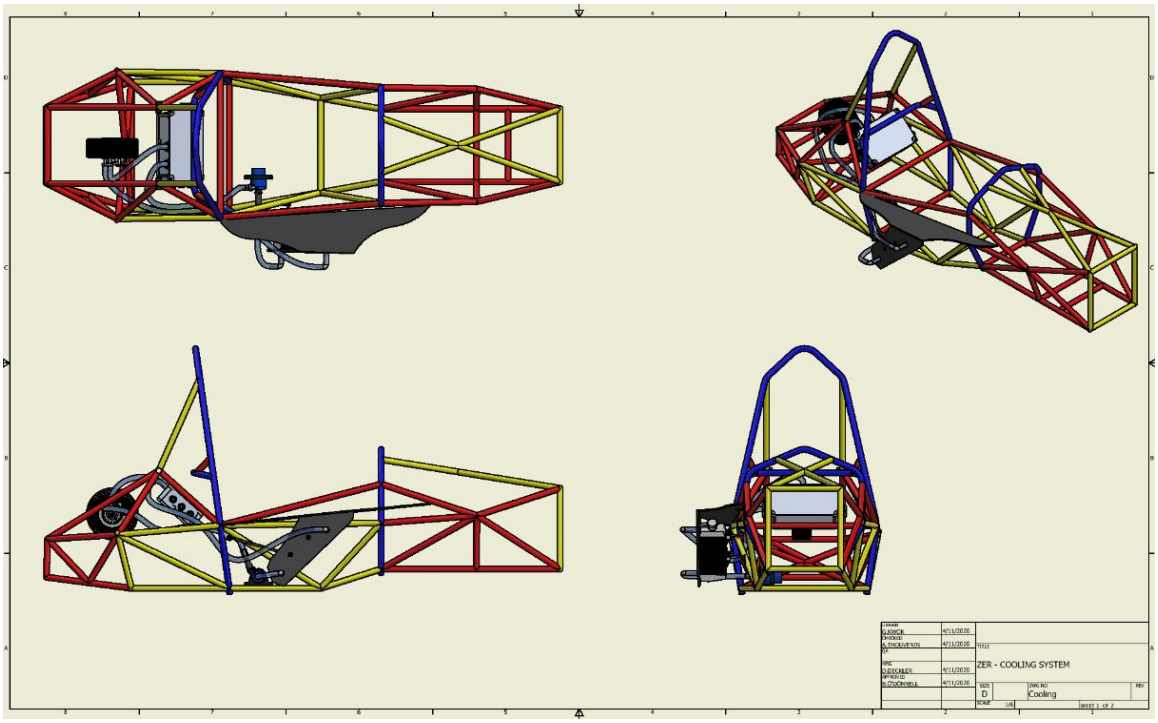

Figure 44. System Assembly Drawing

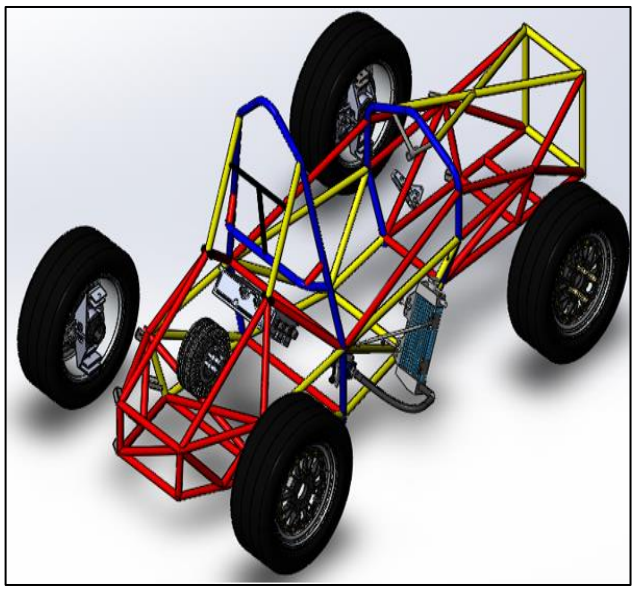

Figure 45. Cooling Subsystem Isometric View

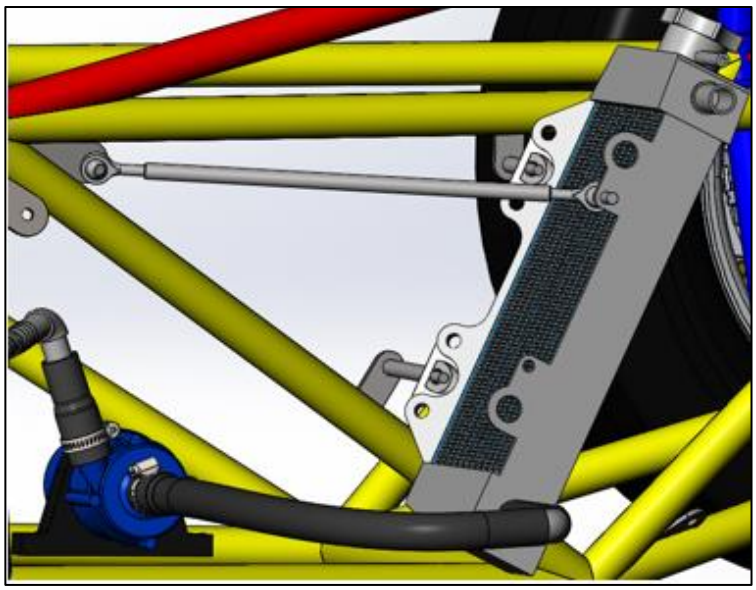

Figure 46. Radiator Mounting Design

4.7 Bill of Materials (BOM)

Table 7. Bill of Materials

BILL OF MATERIALS				
Item No.	**Part**	**Quantity**	**Description/Material**	**Manufacturer/ Distributor**
1	Radiator	1	Mishimoto X-Braced Dirt Bike Radiator	Mishimoto
2	Radiator Cap	1	-	Mishimoto
3	Centrifugal Pump	1	EBP40 12V	Davies Craig
4	Inverter	1	PM100DX	Cascadia Rinehart
5	Electric motor	1	Emrax 228MV	Emrax
6	Catch can	1	Heinmo HM3-TY1LSH-B	Heinmo
7	Tubing (1 ft)	8.5	3/4" ID/ 1" OD - Silicone	McMaster-Carr
8	Motor Hose Barbed Fitting	2	Aluminum	*In-house*
9	Inverter Hose Barbed Fitting	2	Aluminum	*In-house*
10	90° Elbow Connector	3	PVC	McMaster-Carr
11	Straight Connector	1	PVC	McMaster-Carr
12	Check valve	1	PVC	McMaster-Carr
13	Radiator Correction Angle	2	Aluminum	*In-house*
14	Mounting Standoff 1	1	Steel	*In-house*
15	Mounting Standoff 2	1	Steel	*In-house*
16	Mounting Standoff 3	1	Steel	*In-house*
17	Radiator Top Cover	1	Textreme - Carbon Fiber/Composite	*In-house*
18	Radiator Bottom Cover	1	Textreme - Carbon Fiber/Composite	*In-house*
19	Hose Clamp	16	Nylon	McMaster-Carr
20	Bolt	8	Steel - Grade 8.8 (SAE 5)	Fastenal
21	Toplock Nut	8	Steel - Grade 8.8 (SAE 5)	Fastenal
22	Washer	2	Steel - Grade 8.8 (SAE 5)	Fastenal
23	Distilled Water (1 L)	2	-	-

A second BOM, Figure 47, was completed on https://www.fsaeonline.com/ to comply with FSAE requirements and to estimate the cost of a system in a large scale manufacturing environment.

Assembly Cost $219.86
Total $219.86

Parts

	Part	Part #	Op Num	Part Cost	Quantity	Subtotal
1	Radiator	-		40.12	1	40.12
2	Water Pump	-		20	1	20.00
3	Catch Can	-		22.62	1	22.62
4	Tubing	-		18.65	1	18.65
5	Motor Hose Barbed Fitting	-		5.9	2	11.80
6	Inverter Hose Barbed Fitting	-		3.71	2	7.42
7	Tube 90 Degree Elbow Connector	-		0.13	3	0.39
8	Tube Straight Connector	-		0.06	1	0.06
9	Check Valve	-		7	1	7.00
10	Radiator Aluminum Angle	-		4.15	2	8.30
11	Mounting Rod 1	-		5.4	1	5.40
12	Mounting Rod 2	-		6.14	1	6.14
13	Mounting Rod 3	-		5.92	1	5.92
14	Radiator Cover	-		51.67	1	51.67

Subtotal $205.49

Materials

	Material	Use	Op Num	Size 1	Size 2	Area Name	Area	Length	Density	Quantity	Unit Cost	Subtotal
3	Fluid, Coolant			2 L						1	2e-4	

Subtotal $0.00

Processes

	Process	Use	Op Num	Quantity	Multiplier	Mult. Val.	Unit Cost	Subtotal
7	Assemble, 1 kg, Interference	Connect tubing to barbed fittings		10		1	0.19	1.90
8	Screwdriver > 1 Turn	Tighten mounting fasteners		6		1	0.5	3.00

Subtotal $4.90

Fasteners

	Fastener	Use	Op Num	Size 1	Size 2	Quantity	Unit Cost	Subtotal
2	Hose Clamp, Worm Drive	Secure components		15.875 mm		16	0.5635	9.02
3	Nut, Grade 8.8 (SAE 5)	Radiator Mounting		5 mm		6	0.0245	0.15
4	Washer, Grade 8.8 (SAE 5)	Pump Mounting		5 mm		2	0.01	0.02
5	Nut, Grade 8.8 (SAE 5)	Pump Mounting		5 mm		2	0.0245	0.05
6	Bolt, Grade 8.8 (SAE 5)	Radiator mounting		0.25 in	0.5 in	6	0.0366	0.22
7	Bolt, Grade 8.8 (SAE 5)	Pump Mounting		0.25 mm	0.5 mm	2	0.0032	0.01

Subtotal $9.47

Figure 47. Bill of Materials for FSAE Compliance. Retrieved from https://www.fsaeonline.com/

Chapter 5: Discussion

The design considerations for the cooling system of the ZER 2020 racecar spanned almost all the fundamentals of the engineering discipline. Some of these considerations have been discussed in the preceding sections. Besides meeting FSAE rules and maintaining proper heat dissipation, other considerations, such as, fluid mechanics, weight reduction, footprint reduction, error analysis, and financial considerations have also been made.

The placement of the EBP40 centrifugal pump was one hurdle faced by the team. The pump was chosen to be placed immediately following the radiator to ensure that the pump saw the coolest water, thus, keeping the pump in its optimal working conditions. The pump was placed at the lowest point in the system to avoid any chance of cavitation. The total length of tubing and the number of connectors was vastly reduced from the 2019 cooling system design. By reducing the length of tubing, the system was simplified for design, manufacturing, and troubleshooting. Because each connector introduces its own loss coefficient, reducing the number of connectors was a simple way to optimize the system by minimizing pressure loss. In addition to these benefits, minimizing the footprint of the tubing loop reduced the amount of water needed to run the system, thus, reducing weight.

Because of the nature of the vehicle and its purpose, extra attention was given to reducing the footprint of the cooling system. The small frame of the vehicle had to accommodate a large accumulator, motor, and inverter while following FSAE guidelines for safety. The cooling system was designed to be as compact as possible to allow for increased design possibilities for the remaining Zips Electric Racing subsystems. Budgeting and financial goals were also included in the design process with the goal being to produce an optimal system at a low cost.

Chapter 6: Conclusion

A cooling system is an essential component of the Zips Electric Racecar as without it, the car can exceed its maximum operating temperatures, potentially resulting in damaging components. The final design successfully incorporated the pre-selected, system critical, components and optimizing the overall system in the process.

Testing of the system critical components in the wind tunnel resulted in a better understanding of the thermal fluid characteristics of the system. The data analysis along with the theoretical analysis and simulations solidified the team’s confidence in a functional system, as well as expanded the teams knowledge of analyzing and predicting the characteristics of such systems.

The final design of the cooling system was optimized around a 70° radiator mounting angle, maximizing the forward-facing surface area, thus increasing the forced convection over the radiator find. Also, the pump was placed at the lowest point within the system to decrease the risk of cavitation, increasing the pump efficiency. These manufacturing requirements, along with the thermal fluid analysis and simulations, would allow the Zips Electric Racecar to operate continuously, under normal conditions, during competition.

References

"2020 Rules and References." *Formula SAE,* https://www.fsaeonline.com/cdsweb/gen/DownloadDocument.aspx?DocumentID=1b6bda52-48d0-4286-931d-c9418165fd3e

"Density of Selected Solids." *The Engineering Toolbox,* https://www.engineeringtoolbox.com/density-solids-d_1265.html

Bergman, T.L., Lavine, A.S., Incropera, F.P., Dewitt, D.P. (2011). *Introduction to Heat Transfer* (6th ed.). Jefferson City, Wiley.

Gerhart, P.M., Gerhart, A.L., & Hochstein, J.I. (2016). *Munson, Young, and Okiishi's Fundamentals of Fluid Mechanics* (8th ed.). Hoboken, NJ: John Wiley & Sons.

Lienhard IV, J.H., & Lienhard V, J.H. (2017). *A heat transfer textbook* (4th ed.). Cambridge, MA: Phlogiston Press.

Appendix A – MATLAB Code

Analysis

```
% 8 L/min - Constant T_in (Open Loop)
% Water Properties at 27C (300K)
clc, clear, close all
rho = 996.5         ; %[kg/m^3] Water Density
cp = 4181           ; %[J/kg.k] Specific Heat
k = 0.6103          ; %[W/m.K] Thermal Conductivity
alpha = 1.465e-7    ; %[m^2/s] Thermal Diffusivity
nu = 8.568e-7       ; %[m^2/s] Kinematic Viscosity
Pr = 5.85           ; %[-] Prandtl's Number
beta = 2.75e-4      ; %[1/K] Coefficient of Expansion

Qv = 8 / 60              ; %[L/s] Volumetric Flow Rate
mdot = Qv * rho / 1000   ; %[kg/s] Mass Flow Rate

[mph10, mph20, mph30, mph40, mph50] = Q_8 ; %Data Set

t_10 = mph10(:,1)       ; %[sec] Time stamp for 10mph run
t_20 = mph20(:,1)       ; %[sec] Time stamp for 20mph run
t_30 = mph30(:,1)       ; %[sec] Time stamp for 30mph run
t_40 = mph40(:,1)       ; %[sec] Time stamp for 40mph run
t_50 = mph50(:,1)       ; %[sec] Time stamp for 50mph run

%
% 'F_K' Function File Converts F to K
% Columns 2:5 are: 2:Ambient | 3:RadSurface | 4:Inlet | 5:Outlet
%
% Output Columns are: 1:Ambient | 2:RadSurface | 3:Inlet | 4:Outlet

T_10 = F_K(mph10(:,2:5)); %[K] Temps for 10mph
T_20 = F_K(mph20(:,2:5)); %[K] Temps for 20mph
T_30 = F_K(mph30(:,2:5)); %[K] Temps for 30mph
T_40 = F_K(mph40(:,2:5)); %[K] Temps for 40mph
T_50 = F_K(mph50(:,2:5)); %[K] Temps for 50mph

%
% Change in Temp (Inlet - Outlet)
% Reference Matrix, T_x0 Columns:
% 1:Ambient | 2:RadSurface | 3:Inlet | 4:Outlet
%
% Output Columns are Inserted to T_x0 Matrix:
% 1:Ambient | 2:RadSurface | 3:Inlet | 4:Outlet | 5:dT

T_10(:,5) = T_10(:,3) - T_10(:,4)  ; %[C] dT for 10mph
T_20(:,5) = T_20(:,3) - T_20(:,4)  ; %[C] dT for 20mph
T_30(:,5) = T_30(:,3) - T_30(:,4)  ; %[C] dT for 30mph
T_40(:,5) = T_40(:,3) - T_40(:,4)  ; %[C] dT for 40mph
T_50(:,5) = T_50(:,3) - T_50(:,4)  ; %[C] dT for 50mph

%
```

```
% Isolating Steady State Values Using 'Steady' Function and inserting
% normalized time array for each condition :
% 1:Time | 2:Ambient | 3:RadSurface | 4:Inlet | 5:Outlet | 6:dT

[T_10, dTavg10] = Steady(T_10)      ; % SS for 10mph
[T_20, dTavg20] = Steady(T_20)      ; % SS for 20mph
[T_30, dTavg30] = Steady(T_30)      ; % SS for 30mph
[T_40, dTavg40] = Steady(T_40)      ; % SS for 40mph
[T_50, dTavg50] = Steady(T_50)      ; % SS for 50mph

figure()
plot(T_10(:,1),T_10(:,6),T_20(:,1),T_20(:,6),T_30(:,1),T_30(:,6),T_40(:,1),T_40(:,6),T_50(:,1),T_
50(:,6))
legend('10mph','20mph','30mph','40mph','50mph','Location','SouthEast')
xlabel('Time [s]')
ylabel('dT [C]')
title('Comparison of dT with Velocity')
axis([10 60 0 8])

%
% Calculate Rate of Heat Transfer, Qdot

Q(1) = mdot * cp * dTavg10 / 1000       ; %[kW] Heat Transfer for 10mph
Q(2) = mdot * cp * dTavg20 / 1000       ; %[kW] Heat Transfer for 20mph
Q(3) = mdot * cp * dTavg30 / 1000       ; %[kW] Heat Transfer for 30mph
Q(4) = mdot * cp * dTavg40 / 1000       ; %[kW] Heat Transfer for 40mph
Q(5) = mdot * cp * dTavg50 / 1000       ; %[kW] Heat Transfer for 50mph

V = [10 20 30 40 50]        ; %[mph]
figure()
plot(V,Q)
title('Heat Transfer vs. Air Speed')
xlabel('Wind Speed [mph]')
ylabel('Heat Transfer [kW]')

%
% Change in Temp (Inlet - Ambient)
% For Log Mean Temperature Difference
% Reference Matrix, T_x0 Columns:
% 1:Ambient | 2:RadSurface | 3:Inlet | 4:Outlet
%
% Output Columns are: 1:dT(in-out) | 2:dT(in-am)

dT_10(:,1) = T_10(:,4) - T_10(:,2)  ; %[C] dT for 10mph
dT_20(:,1) = T_20(:,4) - T_20(:,2)  ; %[C] dT for 20mph
dT_30(:,1) = T_30(:,4) - T_30(:,2)  ; %[C] dT for 30mph
dT_40(:,1) = T_40(:,4) - T_40(:,2)  ; %[C] dT for 40mph
dT_50(:,1) = T_50(:,4) - T_50(:,2)  ; %[C] dT for 50mph

%
% Change in Temp (Outlet - Ambient)
% For Log Mean Temperature Difference
% Reference Matrix, T_x0 Columns:
% 1:Ambient | 2:RadSurface | 3:Inlet | 4:Outlet
```

```
%
% Output Columns are: 1:dT(in-out) | 2:dT(in-am) | 3:dT(out-am)

dT_10(:,2) = T_10(:,5) - T_10(:,2)  ; %[C] dT for 10mph
dT_20(:,2) = T_20(:,5) - T_20(:,2)  ; %[C] dT for 20mph
dT_30(:,2) = T_30(:,5) - T_30(:,2)  ; %[C] dT for 30mph
dT_40(:,2) = T_40(:,5) - T_40(:,2)  ; %[C] dT for 40mph
dT_50(:,2) = T_50(:,5) - T_50(:,2)  ; %[C] dT for 50mph

%
% Calculate Log Mean Temperature Difference (LMTD)

LMTD_10 = (max(dT_10(:,2)) - max(dT_10(:,1))) / log(max(dT_10(:,2)) / max(dT_10(:,1)));
LMTD_20 = (max(dT_20(:,2)) - max(dT_20(:,1))) / log(max(dT_20(:,2)) / max(dT_20(:,1)));
LMTD_30 = (max(dT_30(:,2)) - max(dT_30(:,1))) / log(max(dT_30(:,2)) / max(dT_30(:,1)));
LMTD_40 = (max(dT_40(:,2)) - max(dT_40(:,1))) / log(max(dT_40(:,2)) / max(dT_40(:,1)));
LMTD_50 = (max(dT_50(:,2)) - max(dT_50(:,1))) / log(max(dT_50(:,2)) / max(dT_50(:,1)));
```

Functions

```
% Isolate Steady State Region of Data, dT (Tin-Tout) MUST be LAST Column
% Taking Data Points for dT < 8K and creating a new time array 't'
% Calculating Mean dT Value 'B'

function [A, B] = Steady(A)

% A = A .* (A>=1&A(:,length(A(1,:)))<= INPUT dT Constraint Here) ;

A = A .* (A>=1&A(:,length(A(1,:)))<= 8) ;
v = nonzeros(A');
A = reshape(v,5,length(v)/length(A(1,:)))';

t = (0:0.5:(length(A)-1)/2)' ;

A = [t A] ;

B = mean(A(:,length(A(1,:))));

end

function T = F_K(F)

T = (F - 32) * 5 / 9 + 273.15;

end
```

Published with MATLAB® R2019b

Wind Tunnel data tables required to run code is not included

Appendix B – Selected Relevant Equations

For many applications, it is convenient to express the net radiation heat exchange in the form

$$q_{\text{rad}} = h_r A(T_s - T_{\text{sur}}) \tag{1.8}$$

Figure B. 1 – Taken from 'Introduction to Heat Transfer' p. 10

$$q = \dot{m} c_p (T_{\text{out}} - T_{\text{in}}) \tag{1.12e}$$

Figure B. 2 – Taken from 'Introduction to Heat Transfer' p. 496

When the flow is uniformly distributed over the opening in the control surface (one-dimensional flow),

$$\dot{m} = \rho A V$$

Figure B. 3 – Taken from 'Munson, Young, and Okiishi's Fundamentals of Fluid Mechanics' p. 205